RSC Advances

REVIEW

Cite this: *RSC Adv.*, 2022, **12**, 8228

Recent developments in alginate-based adsorbents for removing phosphate ions from wastewater: a review

Abdelazeem S. Eltaweil, *[a] Eman M. Abd El-Monaem,[a] Hala M. Elshishini,[b] Hisham G. El-Aqapa,[a] Mohamed Hosny,[c] Ahmed M. Abdelfatah,[c] Maha S. Ahmed,[d] Eman Nasr Hammad,[e] Gehan M. El-Subruiti,[a] Manal Fawzy[c] and Ahmed M. Omer*[f]

The huge development of the industrial sector has resulted in the release of large quantities of phosphate anions which adversely affect the environment, human health, and aquatic ecosystems. Naturally occurring biopolymers have attracted considerable attention as efficient adsorbents for phosphate anions due to their biocompatibility, biodegradability, environmentally-friendly nature, low-cost production, availability in nature, and ease of modification. Amongst them, alginate-based adsorbents are considered one of the most effective adsorbents for removing various types of pollutants from industrial wastewater. The presence of active COOH and OH^- groups along the alginate backbone facilitate its physical and chemical modifications and participate in various possible adsorption mechanisms of phosphate anions. Herein, we focus our attention on presenting a comprehensive overview of recent advances in phosphate removal by alginate-based adsorbents. Modification of alginate by various materials, including clays, magnetic materials, layered double hydroxides, carbon materials, and multivalent metals, is addressed. The adsorption potentials of these modified forms for removing phosphate anions, in addition to their adsorption mechanisms are clearly discussed. It is concluded that ion exchange, complexation, precipitation, Lewis acid–base interaction and electrostatic interaction are the most common adsorption mechanisms of phosphate removal by alginate-based adsorbents. Pseudo-2nd order and Freundlich isotherms were figured out to be the major kinetic and isotherm models for the removal process of phosphate. The research findings revealed that some issues, including the high cost of production, leaching, and low efficiency of recyclability of alginate-based adsorbents still need to be resolved. Future trends that could inspire further studies to find the best solutions for removing phosphate anions from aquatic systems are also elaborated, such as the synthesis of magnetic-based alginate and various-shaped alginate nanocomposites that are capable of preventing the leaching of the active materials.

Received 20th December 2021
Accepted 28th February 2022

DOI: 10.1039/d1ra09193j

rsc.li/rsc-advances

1. Introduction

Water is "one of Nature's precious gifts to mankind". All organisms from tiny insects to blue whales need this universal solvent to remain alive. In addition, the human body cannot survive without water for over three days. Although we all have to be conscious of the imperative need for water conservation,[1–5] the aggravation of water pollution has grown day by day.[6–9] This catastrophic problem results from the disposal of numerous pollutants into water bodies,[10,11] particularly phosphate owing to its presence in nature and excessive uses in various fields.[12] It is well known that the majority of phosphorus is wrapped up in rocks and sediments.[13] But anthropogenic sources (Fig. 1a) surpass these natural sources, including industrial wastewater, sewage outfall, marine dumping and leakage from underground storage.[14,15] Nonetheless, phosphate reaching water bodies with a concentration above the acceptable level causes eutrophication, leading to significant environmental disruption.[16–18] Eutrophication results in the depletion of dissolved oxygen, which severely affects aquatic organisms that are sensitive to low levels of dissolved oxygen.[19,20] On the other hand, phosphate adversely affects human health, causing damage to bones, blood cells and the liver, kidney failure, and problems to the intestines and circulatory system.[18] Therefore, the maximum amount of phosphate allowed in drinking water

[a]*Chemistry Department, Faculty of Science, Alexandria University, Alexandria, Egypt. E-mail: abdelazeemeltaweil@alexu.edu.eg*
[b]*Department of Environmental Studies, Institute of Graduate Studies and Research, Alexandria University, 163, Horrya Avenue, Alexandria, Egypt*
[c]*Green Technology Group, Environmental Sciences Department, Faculty of Science, Alexandria University, 21511, Alexandria, Egypt*
[d]*Higher Institute of Science and Technology-King Mariout, Egypt*
[e]*Chemistry Department, Faculty of Science, Menoufia University, Egypt*
[f]*Polymer Materials Research Department, Advanced Technology and New Materials Research Institute (ATNMRI), City of Scientific Research and Technological Applications (SRTA-City), P. O. Box: 21934, New Borg El-Arab City, Alexandria, Egypt*

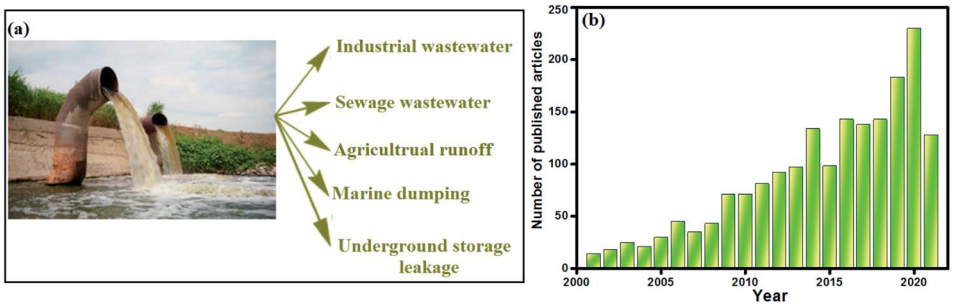

Fig. 1 (a) Sources of phosphate pollution and (b) Scopus database regarding the numbers of published articles about the removal of phosphate from 2001 to 2021.

by the World Health Organization is 5 ppm.[21,22] Consequently, an immense amount of research has been accomplished for removing this detrimental contaminant from wastewater, as represented in Fig. 1b. Diversified treatment techniques have been sustainably evolved for the efficacious removal of phosphate from wastewater, such as catalytic reduction,[23] chemical precipitation,[24] electrocoagulation,[24,25] electrodialysis,[26] membranes,[27] and ion exchange.[28] In addition, the adsorption technique is the most popular mode of remediation due to its design versatility,[29] lack of treatment by-products, ease of service,[30] high efficacy,[31] reusability,[32] low cost, ease of operation, and insensitivity to biological materials in aqueous environments.[33–38]

Numerous materials have been applied as adsorbents for the removal of phosphate, including clays, biochar, red mud, metal oxides, layered double hydroxides, cross-linked hydrophilic biopolymers, activated carbon residue, mesoporous silica spheres, lanthanum-based materials, metal–organic frameworks and nanomaterials.[39–50] Among these adsorbents, natural biopolymers are polymeric organic molecules derived from renewable sources such as algae, the exoskeletons of crustaceans and shells,[51] plants, microbial biomass, and animals, as depicted in Fig. 2. Biopolymers are made up of monomeric sections that are covalently bound together to form larger molecules.[52,53]

Owing to the exceptional structural and physical properties, availability, biocompatibility, and biodegradability of biopolymers, they represent a highly promising choice for the generation of sustainable materials with enhanced adsorption behavior.[54–57] Consequently, biopolymer-based adsorbents have exhibited fabulous adsorption behavior not only toward phosphates but also toward a wide variety of noxious contaminants, including pharmaceuticals,[51] hydrocarbons,[58] pesticides,[59] fluoride,[60] nitrate,[61] heavy metals,[62,63] dyes[64] and nitro-aromatic compounds.[65] Amongst these brilliant biopolymers, anionic alginate (Alg) is a collective family produced from algae and bacteria at a comparatively low cost.[66] Alg is a linear anionic polysaccharide that typically consists of 1,4-linked β-D-mannuronic acid and α-L-guluronic acid monomers. Alg was extracted for the first time in 1881 from kelp, then in the 1930s, it was extracted at a large scale from brown algae such as *Laminaria digitata*, *Laminaria japonica*, *Ascophyllum nodosum*, and *Macrocystis pyrifera*.[67] The alginate extraction process involves several steps. First, the initial treatment is to convert

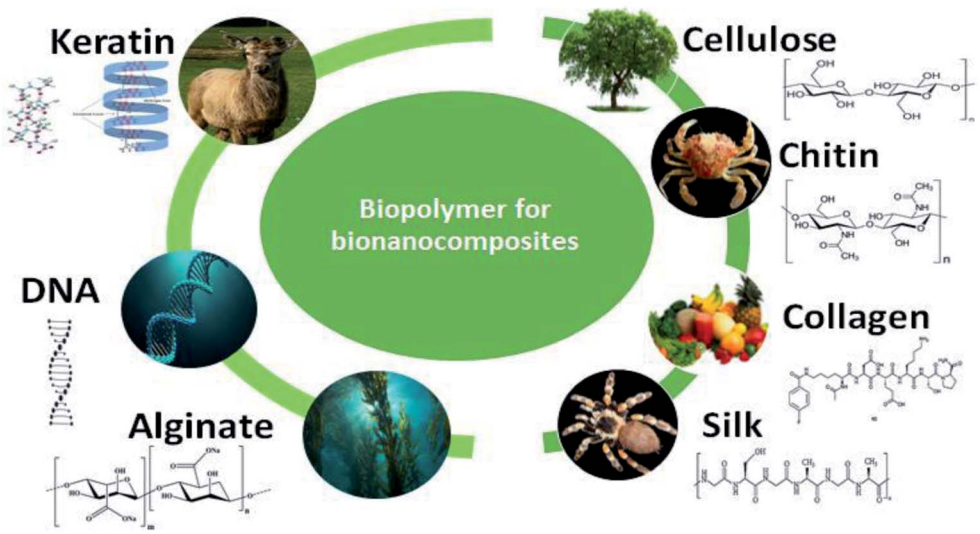

Fig. 2 Various types of biopolymers.

salts of alginic acid in the algae into free alginic acid. Secondly, this is neutralized by sodium carbonate/hydroxide to form water-soluble sodium alginate. Finally, the soluble alginate is recovered *via* precipitation by calcium chloride to form calcium alginate that is later treated with sodium carbonate to produce sodium alginate.[68] Notably, there are many alginate-based salts, including calcium alginate, potassium alginate, and ammonium alginate; however, sodium alginate is the most popular salt.[69,70]

Alginate demonstrates several unique and desirable properties, such as high chemical stability,[71] biocompatibility, biodegradability,[72] nontoxicity, low-cost manufacture,[73] mild gelation, and chelating ability.[74] Accordingly, alginate has been effectively applied in diverse applications, in medical, pharmaceutical, industrial, food, and water treatment sectors (Fig. 3).[30,65,75–77]

Alginate has been extensively used for the removal of noxious anions, as described in the following sections.

It has been reported that alginate-based adsorbents demonstrated acceptable adsorption aptitudes towards various pollutants comprising heavy metals, toxic organic dyes, pharmaceutical residues, aromatic compounds, and other anions such as nitrates and phosphates.[78,79] As a type of water-soluble biopolymer, alginate possesses plenty of functional hydrophilic OH and COOH groups in its structure, which simplifies its physical and chemical reactions. Enormous numbers of modifications have been conducted, such as grafting, crosslinking, composite formation, and surface functionalization by other active groups to boost the adsorption characteristics of native alginate. Hence, this review sums up recent progress in the removal of phosphate from wastewater by alginate-based adsorbents. Various modification approaches are discussed, including the incorporation of clays, carbon materials, layered double hydroxides, metal ions, and magnetic materials into the alginate matrix. The morphology, and chemical and physical properties of the developed alginate adsorbent are clarified based on various characterization tools. Furthermore, the key adsorption parameters that control the phosphate adsorption efficacy onto alginate-based adsorbent are explained. Importantly, the proposed adsorption mechanisms of phosphate ions are thoroughly discussed.

2. Alginate-based adsorbents

2.1. Clay-modified alginate

Clay minerals, such as montmorillonite (Mt), bentonite (BT), and kaolin (KN), are widely used in water treatment applications due to their high specific surface area, low cost, nontoxicity, and availability in many natural sources.[80,81] Hence, the intercalation of clay minerals into alginate enhances its adsorption property. From this perspective, Das *et al.*[82] fabricated montmorillonite–iron crosslinked alginate beads (MtIAlg) for removing phosphate ions from wastewater (Fig. 4). It was found that the removal percent of MtIAlg beads (96%) surpassed that of pure Alg (92%) which may be ascribed to the abundant hydroxyl groups on the Mt surface that interact with phosphate. Moreover, the batch study showed that there was no obvious change in the phosphate removal percent with the increase in pH from 2 to 10. This finding indicated that phosphate adsorption onto MtIAlg beads was not greatly affected by electrostatic attraction and the adsorption mechanism was mainly dominated by chemisorption mechanisms. The kinetic study confirmed this result for which the experimental data were a good fit to pseudo-second order model. Besides, the

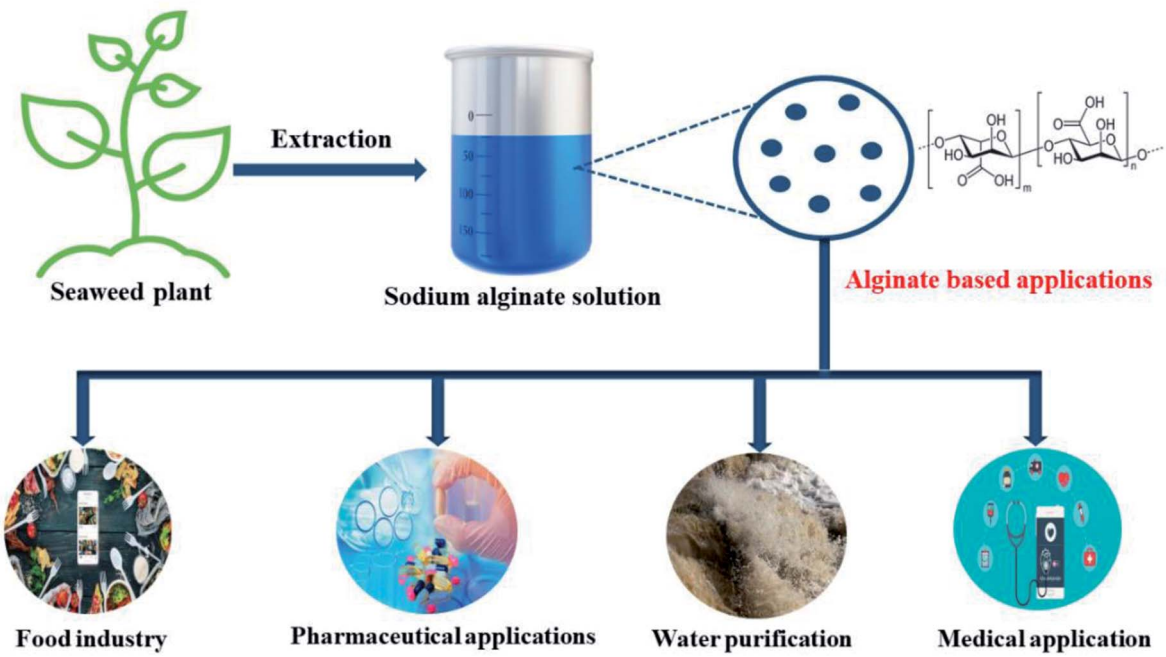

Fig. 3 The extraction of Alg and its applications in diverse fields.

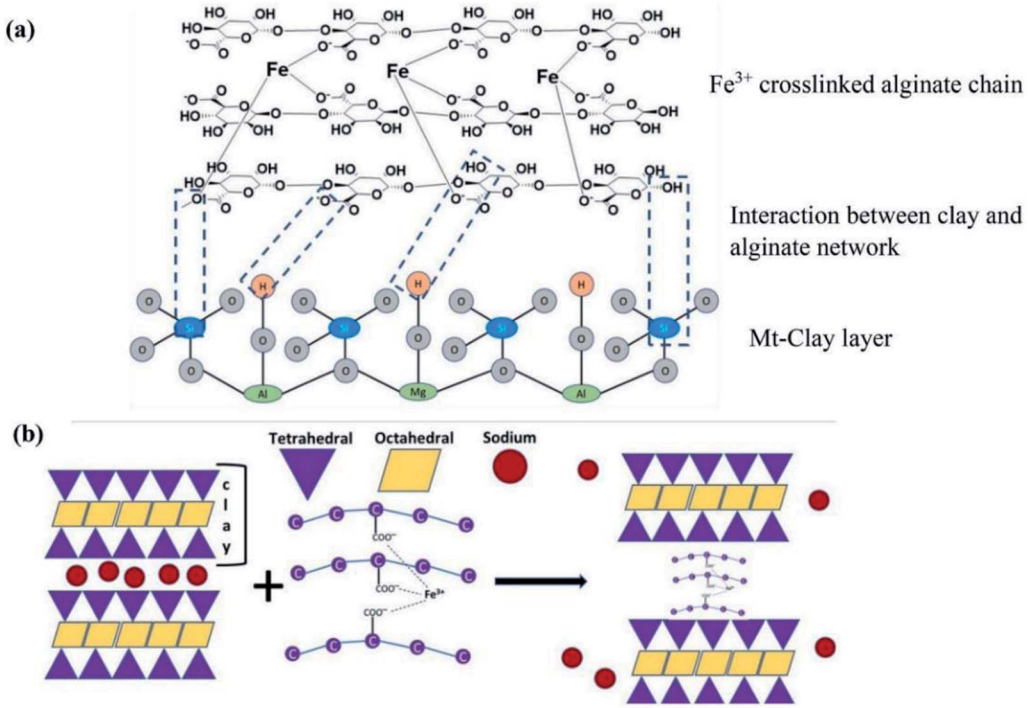

Fig. 4 (a) The crosslinking process of Fe^{3+} to Alg network and interaction with Mt and (b) the possible MtIAlg network configuration. This figure reproduced from ref. 82 with permission from Elsevier. Copyright (2021).

significant decline in the adsorption rate of phosphate over time suggests that the adsorption depends on the diffusion of phosphate ions from their bulk solution to the external surface of MtIAlg and then diffusion into the internal pores. In addition, the phosphate adsorption mechanism could occur *via* ligand exchange between the hydroxyl groups on the surface of Mt-clay and iron oxide and phosphate ions ($H_2PO_4^-$/HPO_4^{2-}). Also, the complexation between phosphate and iron oxide plays the main role in the adsorption process, as clarified by the Fourier transform infrared (FTIR) spectrum of the beads after the adsorption of phosphate.

Kaolin (KN), a silicate clay, consists of different ratios of Al_2O_3, SiO_2, MgO, and CaO. Owing to its ion-exchange ability, thermal stability, binding ability, and high surface area, KN is widely used as a good adsorbent.[83,84] In this regard, Ilango *et al.*[85] prepared zirconium crosslinked alginate/kaolin composite beads (Zr@AlgKN) (Fig. 5a) *via* a hydrothermal method to enhance its adsorbent properties by increasing its surface area. BET results showed that the specific surface area (S_{BET}) of hydro-supported Zr@AlgKN composite beads (78.93 $m^2\ g^{-1}$) was higher than that of *in situ* assisted Zr@AlgKN composite beads (67.15 $m^2\ g^{-1}$). Furthermore, from the scanning electron microscopy (SEM) images (Fig. 5b and c) the particle sizes of *in situ* and hydro-assisted Zr@AlgKN were measured to be 1.597 and 1.362 mm, respectively. It was observed that the incorporation of Zr(IV) on AlgKN composite beads enhanced the adsorption capacity of the composite due to the high affinity of Zr(IV) to phosphate ions. The FTIR spectrum of Zr@AlgKN composite beads after the adsorption of phosphate ions (Fig. 5e) indicated the successful adsorption of phosphate since the characteristic bands were slightly shifted. Moreover, the presence of distinct phosphate ion peaks at 1032 and 560 cm^{-1} provides additional evidence for phosphate ion adsorption. The X-ray diffraction (XRD) of Zr@AlgKN (Fig. 5f) depicted the same crystalline peaks of both KN and Alg, indicating that the structures of KN and Alg were not changed.

Moreover, it was found that the adsorption of phosphate reached its peak when the pH increased from 3 to 7 which may be ascribed to the electrostatic interaction between positive charges on the Zr@AlgKN ($pH_{pzc} = 5.64$) and phosphate ions. In contrast, at pH above 7, the beads were negatively charged and surrounded by hydroxyl groups which could compete with phosphate ions for the active sites of the beads. This result agrees well with the studies by Youness *et al.*,[86,87] and Qixuan *et al.*[88] The adsorption of phosphate on Zr@AlgKN composite beads was evaluated in the presence of different co-anions, such as Cl^-, HCO_3^-, SO_4^{2-}, F^- and $HCrO_4^-$. It was found that HCO_3^- showed the lowest competition with phosphate ions for the adsorption sites of the beads. While SO_4^{2-} exhibited the highest competing effect on phosphate adsorption because it has high reactivity and electronic charge.

Recently, bentonite (BT) has drawn a great deal of interest as an applicable adsorbent since it is inorganic.[89] In this context, Xu *et al.*[74] scrutinized the adsorption performance of modified bentonite entrapped in Alg beads (Al–NaBT–Alg) towards the adsorptive removal of phosphate from wastewater. SEM images (Fig. 6a–d) showed a change in the Al–NaBT structure from lamellar to a porous surface with an internal network structure after encapsulation within Alg beads, reflecting an increase in the available adsorption sites. The isotherm study clarified that

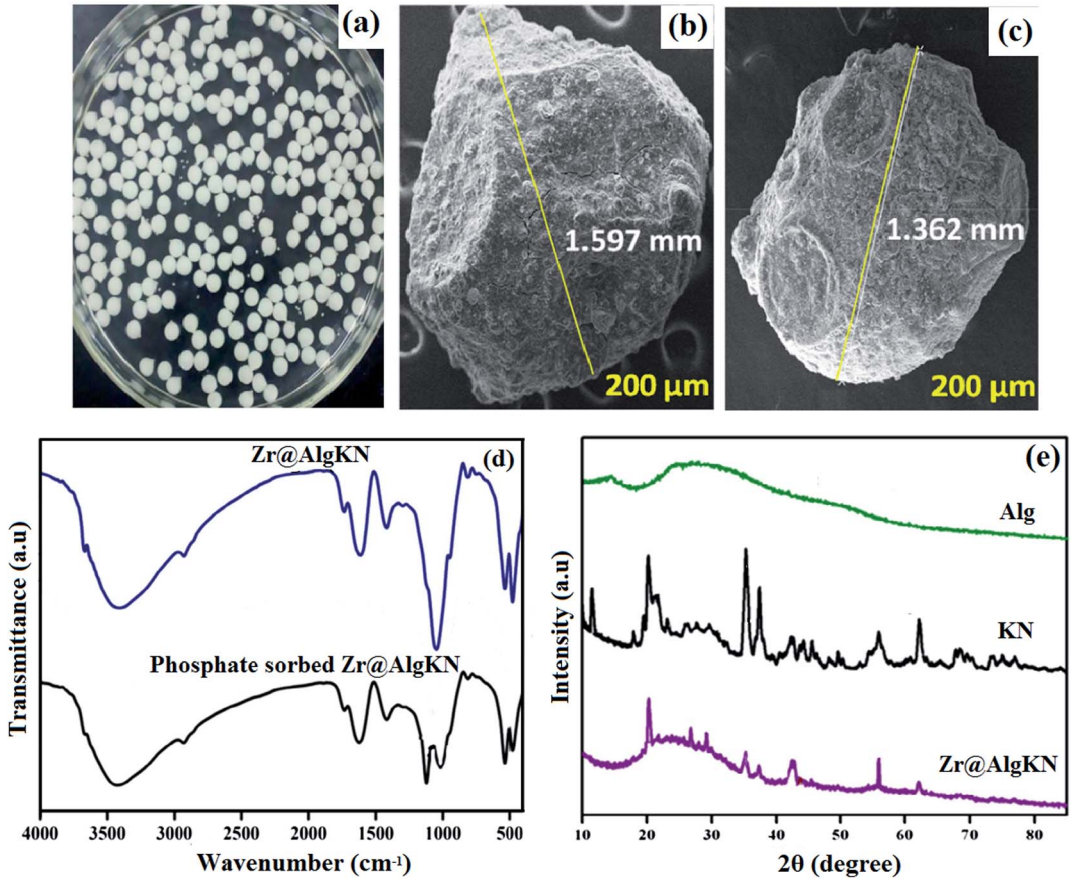

Fig. 5 (a) Digital image for Zr@AlgKN, (b) SEM of Zr@AlgKN (*in situ*), (c) SEM of Zr@AlgKN (hydro), (d) FTIR spectra of Zr@AlgKN before and after the adsorption of phosphate, and (e) XRD patterns of Alg, KN and Zr@AlgKN. This figure reproduced from ref. 85 with permission from Elsevier. Copyright (2020).

the adsorption of phosphate ions onto Al–NaBT–Alg beads obeyed the Sips model and the maximum adsorption capacity (q_{max}) was 15.77 mg g^{-1}. Furthermore, the kinetics study revealed that the adsorption process best fitted intra-particle diffusion and film diffusion with three different steps. In the first step, the ions diffused from the bulk solution to the external surface of the beads. While the second step involved transferring the ions from the surface into the beads and the third step represented the equilibrium. It was postulated that the adsorption mechanism (Fig. 6e) of phosphate onto the fabricated beads was controlled by ligand exchange between $H_2PO_4^-$ and OH^- on the surface of the beads and anion exchange between $H_2PO_4^-$ ions and anions (*viz.*, Cl^- and OH^-) as elucidated in the following equations:

$$R–OH + H_2PO_4^- \rightarrow R–H_2PO_4 + OH^- \quad (1)$$

$$R–OH + R–Cl + 2H_2PO_4^- \rightarrow 2R–H_2PO_4 + OH^- + Cl^- \quad (2)$$

In another attempt, Xi *et al.*[90] studied the removal of phosphate from an aqueous medium using Alg–MgO@BT composite beads. Two different ways of drying were used to prepare two kinds of beads: freeze-drying (Alg–MgO@BT) and oven drying (OAlg–MgO@BT). It was found that the S_{BET} of Alg–MgO@BT, OAlg–MgO@BT, and Alg–BT were 59.5, 42.9, and 26.8 $m^2 g^{-1}$ and the pore volumes were 0.135, 0.126, and 0.066 $cm^3 g^{-1}$, respectively. This finding evinced that MgO improved the S_{BET} and the pore volume of Alg–BT beads. This result was consistent with the cross-sectional images of Alg–BT, Alg–MgO@BT, and OAlg–MgO@BT which showed that Alg–MgO@BT and OAlg–MgO@BT possess more abundant mesopores than Alg–BT, implying that MgO provided more adsorption sites. It was observed that Alg–MgO@BT has enhanced adsorption capacity over OAlg–MgO@BT which may be attributed to the higher porosity of the freeze-dried beads. Furthermore, phosphate adsorption onto Alg–MgO@BT increased from 58% to 99% with an increase in the concentration of MgO from 0.05 to 0.2 mol L^{-1}, respectively. It was concluded that MgO provided more active sites which agrees with Lihua *et al.*[91] One of the difficulties of phosphate removal is its presence in multiple forms where it exists as H_3PO_4 (pH < 2), $H_2PO_4^-$ (pH 2–7), HPO_4^{2-} (pH 7–11), and PO_4^{3-} (pH > 11). Alg–MgO@BT showed a high adsorption capacity towards phosphate ions over a wide pH range (3–10) where the phosphate removal efficiency exceeded 99% at a pH lower than 7. This may be anticipated from the strong electrostatic interaction between $H_2PO_4^-$ and HPO_4^{2-} species and the positively charged Alg–MgO@BT. In addition there is a possibility of these species exchanging with the hydroxyl groups on the surface of the beads,

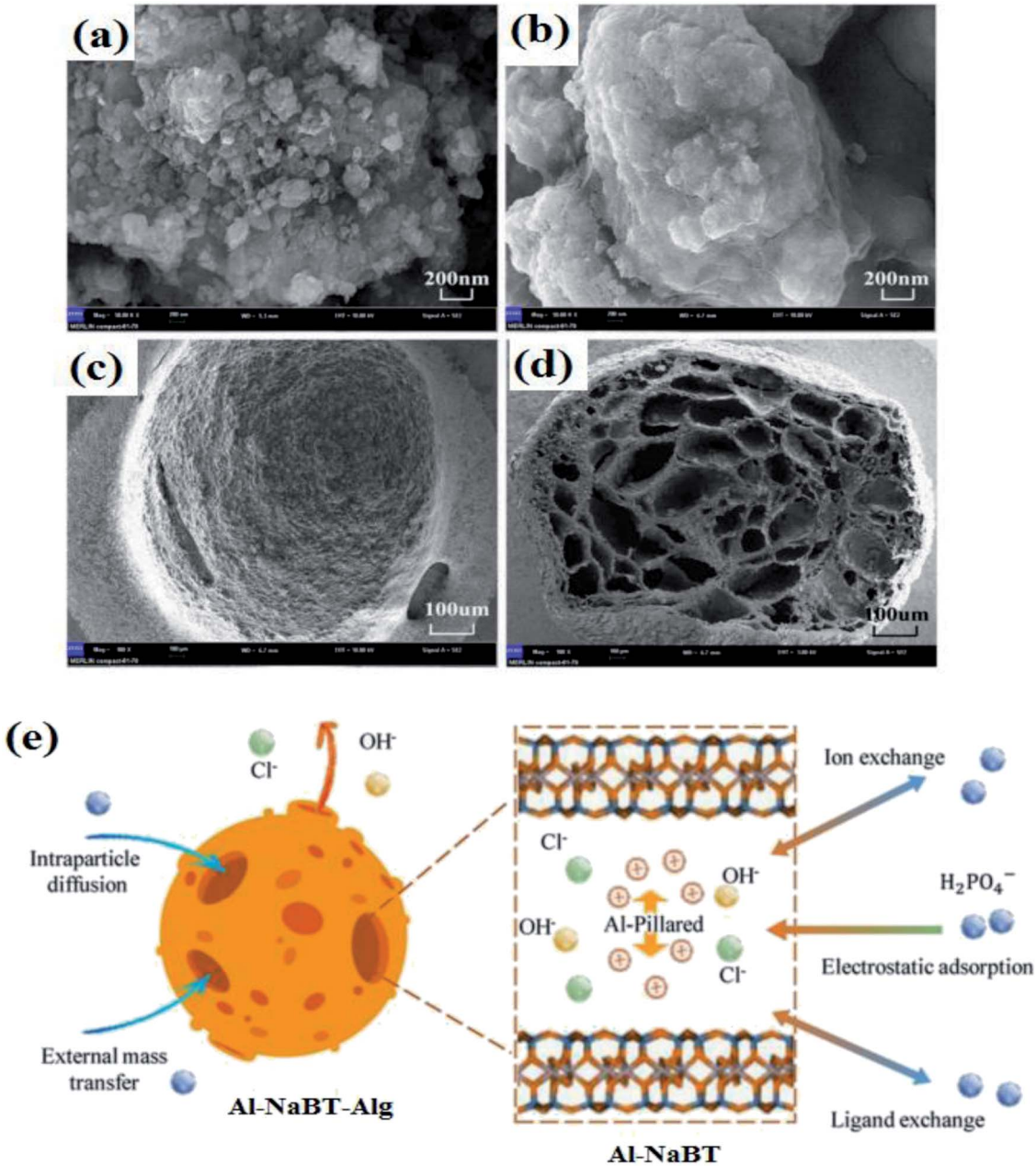

Fig. 6 (a) SEM image of Al–NaBT powder, (b and c) the surface of Al–NaBT–Alg beads, (d) the cross-section of Al–NaBT–Alg beads, and (e) a schematic representation for the possible adsorption mechanisms of phosphate onto Al–NaBT–Alg beads. This figure reproduced from ref. 74 with permission from Elsevier. Copyright (2020).

as shown in Fig. 7. Furthermore, by comparing XPS (X-ray photoelectron spectroscopy) before and after the adsorption of phosphate ions, the Mg-spectrum showed that MgO formed a complex with phosphate since the peaks characteristic of Mg–P appeared and the peak area of M–O decreased, suggesting that MgO contributed greatly to the adsorption process. Moreover, the removal efficiency of phosphate ions was tested in the presence of interfering ions such as Cl^-, SO_4^{2-}, NO_3^-, HCO_3^- and F^-. HCO_3^- and F^- showed the highest negative effect on the removal efficiency owing to their high affinity to MgO and ability to bond to Alg–MgO@BT with electrostatic attraction. In contrast, Cl^- and NO_3^- had a negligible effect on the removal efficiency of phosphate due to their weak binding to the outer surface of Alg–MgO@BT.[90]

In another study, Huan *et al.*[92] synthesized alginate-immobilized Zr–BT hydrogel beads (NH–Alg–ZrBT). These beads were modified by using the Na_2CO_3/HCl pore-forming technique to enhance the adsorption capacity of the fabricated beads toward phosphate ions, as shown in Fig. 8. SEM images depicted that both NH–Alg–ZrBT and NH–Alg–BT have a porous structure due to the reaction between Na_2CO_3 and HCl and the release of CO_2 according to the following equation:

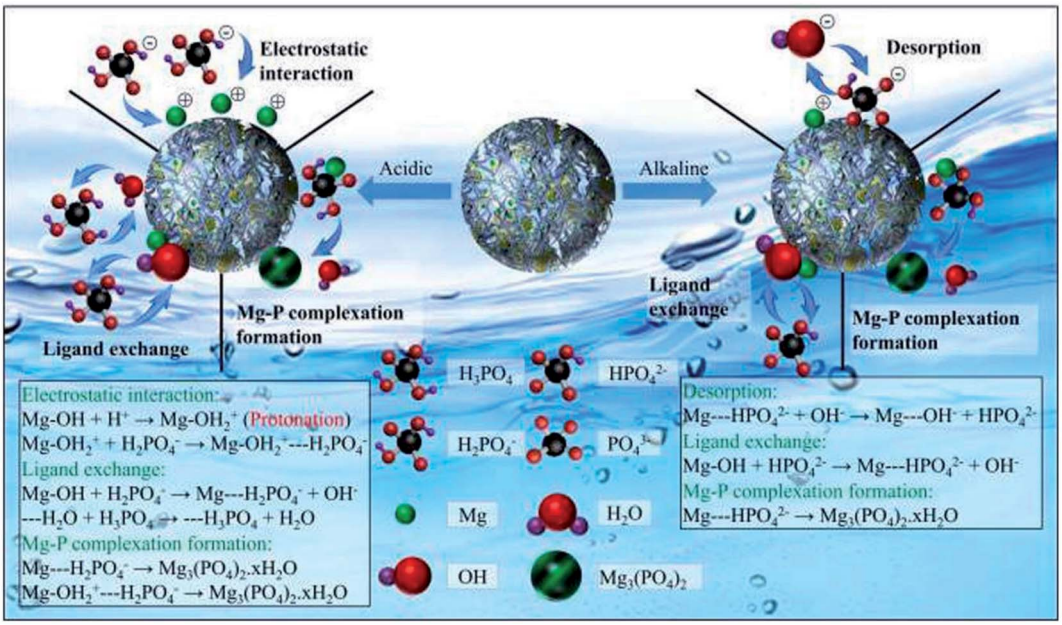

Fig. 7 The multiple forms of phosphate ions and the possible mechanism to adsorb phosphate ions onto Alg–Mgo@BT. This figure reproduced from ref. 90 with permission from Elsevier. Copyright (2021).

$$Na_2CO_3 + 2HCl \rightarrow 2NaCl + H_2O + CO_2\uparrow \quad (3)$$

It was found that the S_{BET} of NH–Alg–ZrBT and Alg–ZrBT were 53.83 and 52.39 $m^2\ g^{-1}$, respectively, while NH–Alg–BT showed a lower S_{BET} of 30.43 $m^2\ g^{-1}$, indicating that Zr(IV) plays a significant role in enhancing the S_{BET} of the beads. The pore volumes of NH–Alg–ZrBT (9.97×10^{-2} $cm^3\ g^{-1}$) and NH–Alg–BT (8.66×10^{-2} $cm^3\ g^{-1}$) were larger than that of Alg–ZrBT (5.64 ×

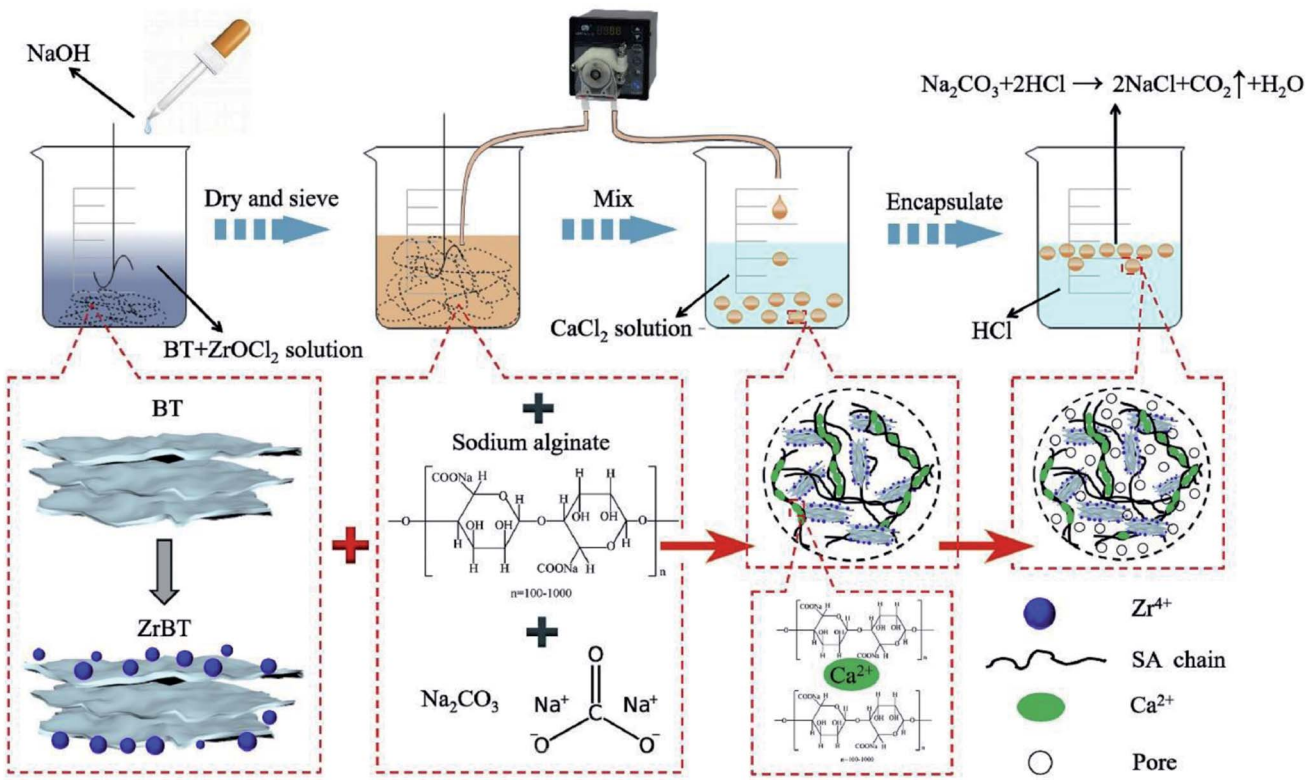

Fig. 8 Illustration of the fabrication process of NH–Alg–ZrBT. This figure reproduced from ref. 93 with permission from Elsevier. Copyright (2021).

10^{-2} cm^3 g^{-1}), proving that the pore-forming process improved the porosity of the beads. This result explained the highest adsorption capacity (42.2 mg g^{-1}) and removal efficiency (94.4%) of NH–Alg–ZrBT.[93]

One more study was intended to develop Alg beads for the efficient removal of phosphate from wastewater.[94] This modification of the alginate depended on (i) the high chemical stability and mechanical strength of polyvinyl alcohol (PVA), (ii) the high affinity of La towards phosphate, and (iii) the high specific surface area and the cation exchange capacity of palygorskite. La/PVA/Alg/Pal beads exhibited a high adsorption capacity toward phosphate ions, reaching 33.20 mg L^{-1} at pH 4 and 25 °C. Furthermore, the selectivity of La/PVA/Alg/Pal beads toward phosphate ions was scrutinized in the presence of coexisting ions, showing that the removal efficiency of phosphate was 100% in the presence of Cl^-, NO_3^-, and SO_4^{2-}. In contrast, F^- exhibited a negative effect on the removal of phosphate due to the high affinity of La towards F^-. Moreover, a kinetics study revealed that the experimental data fitted the pseudo-second order (R^2 = 0.968–0.984), indicating that the adsorption mechanism of phosphate onto La/PVA/Alg/Pal beads was chemisorption. The FTIR spectrum of La/PVA/Alg/Pal beads after the adsorption of phosphate implied the high affinity of La towards phosphate since the distinguishing peak of La–O was shifted from 526 to 514 cm^{-1}. Furthermore, the shifting of the hydroxyl peak from 3398 to 3410 cm^{-1} suggested ligand exchange between hydroxyl groups and phosphate anions.[95] In yet another attempt, Hanna Siwek *et al.*[94] prepared an alginate/goethite hydrogel composite (Alg/α-FeOOH) taking into account the advantages of α-FeOOH, including high mechanical stability, selectivity towards phosphate, and large specific area. To evaluate the mechanical stability of Alg/α-FeOOH, the hydrogel was soaked in deionized water and two different types of natural water (hard and soft water) for 28 days. A slight decrease in the mechanical stability of the soaked hydrogel was noticed in deionized water and soft water. While the mechanical stability of the hydrogel in the hard water declined significantly, owing to the high concentration of Na, K, and Mg in hard water, which contributed to monovalent cation exchange with Alg/α-FeOOH causing the hydrogel to dissolve. Moreover, it was reported that the removal efficiency of phosphate by Alg/α-FeOOH hydrogel was 97.6%. Furthermore, there was no significant change in removal efficiency over a wide pH range (4–9) except for a slight decrease in phosphate removal aptitude (96.3%) at pH 10.[94]

2.2. Magnetic materials-modified alginate

Spinel ferrites have attracted great attention in various applications and in particular in wastewater treatment owing to their

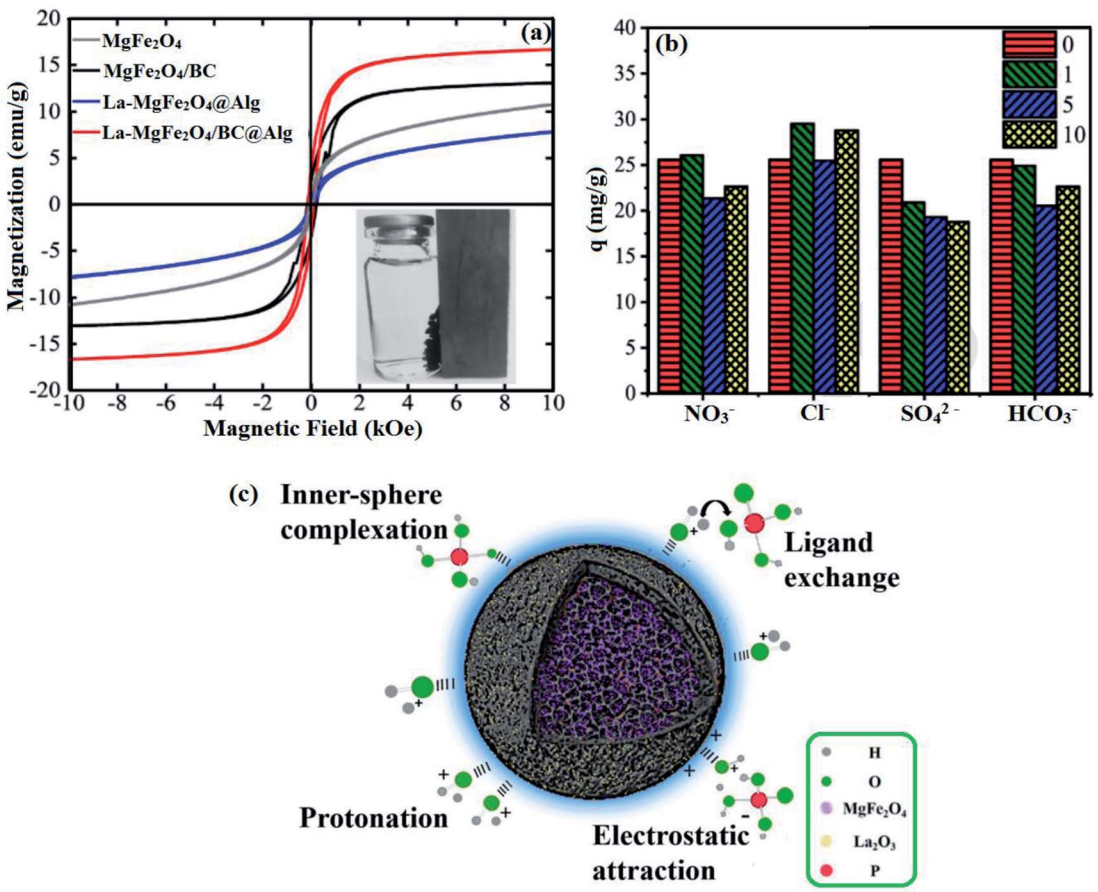

Fig. 9 (a) VSM measurement, (b) effect of different concentrations of coexisting ions on phosphate adsorption, and (c) the proposed adsorption mechanisms of phosphate onto La–$MgFe_2O_4$/BC@Alg. This figure reproduced from ref. 100 with permission from Elsevier. Copyright (2021).

high stability, superparamagnetic behavior, and non-toxicity.[96] One of these ferrites is $MgFe_2O_4$ which showed a high adsorption capacity for many contaminants in water, such as arsenic,[97] lead,[98] phosphate,[96] and dyes.[99] In this context, Li Wang *et al.*[100] studied the removal of phosphate from wastewater by using $MgFe_2O_4$-biochar based lanthanum alginate beads (La–$MgFe_2O_4$/BC@Alg). It was found from a comparison between the XRD patterns of pristine $MgFe_2O_4$ and La–$MgFe_2O_4$/BC@Alg that the beads had the same characteristic peaks as $MgFe_2O_4$ but with higher intensity, indicating that there was no change in $MgFe_2O_4$ structure with an increase in crystallinity. Furthermore, vibrating sample magnetometer (VSM) measurement (Fig. 9a) pointed out that the high saturation magnetization of La–$MgFe_2O_4$/BC@Alg, $MgFe_2O_4$/BC, pristine $MgFe_2O_4$ and La–$MgFe_2O_4$@Alg were 16.16, 13.05, 10.48, and 7.93 emu g^{-1}. This finding proved that BC had a role in dispersing $MgFe_2O_4$ and preventing the aggregation of particles. Moreover, the adsorption capacities of La–$MgFe_2O_4$/BC@Alg, $MgFe_2O_4$, and $MgFe_2O_4$–BC toward phosphate ions were examined. The experimental results showed that the adsorption capacity of phosphate onto La–$MgFe_2O_4$/BC@Alg (26.83 mg g^{-1}) was more than twice those of La–BC@Alg (11.24 mg g^{-1}) and La–$MgFe_2O_4$@Alg (11.80 mg g^{-1}). This implied a synergistic effect between the bead's components. The influence of coexisting ions (NO_3^-, HCO_3^-, SO_4^{2-} and Cl^-) on the adsorption performance of La–$MgFe_2O_4$@Alg towards phosphate ions was assessed (Fig. 9b). The results showed out that SO_4^{2-} exhibited the highest hindrance to phosphate adsorption due to its high negative charge which could be easily attracted to La–$MgFe_2O_4$@Alg. Fig. 9c represents the proposed adsorption mechanism of phosphate onto La–$MgFe_2O_4$/BC@Alg: protonation, electrostatic interaction, ligand exchange, and inner-sphere complexation. The ligand exchange could be proved through XPS analysis where the percentage of M–OH decreased from 83.81 to 62.78%. In addition, M–O increased from 8.48 to 9.21% after phosphate adsorption due to ligand exchange between the hydroxyl groups and phosphate anions, as explained in the following equation:[100]

$$M\text{–}OH_2^+ + H_2PO_4^- \rightarrow \equiv M\text{–}O\text{–}P(OH)_3^+ + OH^- \quad (4)$$

In another attempt, Ilango *et al.*[101] investigated the removal of phosphate by magnetic Fe_3O_4/alginate composite beads which were modified by amine groups to improve their adsorption capacity (Fe_3O_4/Alg@NH_2). It was reported that the calculated q_{max} of phosphate under the Langmuir isotherm was 32.07 mg g^{-1} at 50 °C. The adsorption of phosphate was confirmed by the FTIR spectrum of Fe_3O_4/Alg@NH_2 after the adsorption of phosphate, at which a shift occurred in the bands belonging to OH, NH_2, and Fe_2O_3. Furthermore, the energy-dispersive X-ray (EDX) analysis of Fe_3O_4/Alg@NH_2 after the adsorption process revealed the discriminative peak of phosphate at 2.0 keV with a high percentage (6.82%). It was observed that in a pH range of 2–7, Fe_3O_4/Alg@NH_2 showed a high adsorption capacity, reaching 30.14 mg g^{-1}, which may be attributed to Lewis acid–base interaction of Fe_3O_4 and NH_2 (Lewis acid) and $H_2PO_4^-$ (Lewis base).[101]

This explanation is in line with Huayong *et al.*'s[102] study that suggested the occurrence of the adsorption of phosphate onto Fe_3O_4/PAM/Alg–Zr beads *via* a chemical interaction represented in Lewis acid–base interaction between Zr(IV) and phosphate and ligand exchange, in addition to a physical interaction represented in electrostatic interaction between phosphate ions and Fe_3O_4/PAM/Alg–Zr beads.

2.3. Layered double hydroxide-modified alginate

Layered double hydroxides (LDHs) are a sort of anionic clay with a two-dimensional template structure and permanent positive charge.[103,104] The formula for LDHs could be represented as $[M_{(1-\alpha)}^{2+}N^{3+}(OH)_2]^{\alpha+}[A^{n-}]_{\alpha/n}\cdot mH_2O$ where M^{2+} and N^{3+} are divalent and trivalent metal cations, respectively. While A^{n-} symbolizes the interlayer anion and α is the $N^{3+}/(M^{2+} + N^{3+})$ molar ratio in the range 0.18 to 0.33.[105] Recently, LDHs have received enormous attention and are widely applied in many applications, such as drug delivery,[106] solar cells,[107] gas sensors,[108] catalysis,[109] and especially in wastewater treatment.[110] Indeed, LDHs have promising merits, including large surface area, large interlayer spaces, high anion exchange capacity in the range 2–5 mmol g^{-1}, and flexibility in composition.[111,112] Based on these advantages, LDHs have been used to improve the adsorption property of Alg. However, in limited research involving using an LDHs/Alg composite as an adsorbent, they have exhibited fabulous adsorption performance. In this regard, Han *et al.*[113] fabricated a new composite from Mg–Al LDH/Alg beads (Fig. 10a) to adsorb phosphate ions from wastewater. The high dispersion of Mg–Al LDH powder renders its separation after the adsorption process quite hard. So, the encapsulation of Mg–Al LDH within Alg beads is a fascinating solution to solve its separation problem. Different percentages of Mg–Al LDH were added in Alg beads to investigate the effect on enhancing the removal of phosphate. Monitoring of the removal percent of phosphate by pure Alg beads showed a sharp increase from 14.1% to 86.4% after the incorporation of 2% Mg–Al LDH into the beads. A further increase in the removal percent of phosphate (95.5%) was recorded when the incorporated percent of Mg–Al LDH reached 4%. While a further increase in the LDH incorporated into Alg beads from 6 to 10% led to a slight increase in the removal percent of phosphate from 96.1 to 99.1%. This result indicated the superb adsorption property of Mg–Al LDH. Moreover, the removal efficiency of phosphate by Mg–Al LDH/Alg beads declined slightly from 98.6% to 95.5% when the pH changed from 4.9 to 8.9.[114] This finding was consistent with Lee *et al.*'s[115] study that demonstrated that the removal of phosphate by Mg–Al LDH/mAlg beads was slightly affected by pH when the removal percent of phosphate decreased by 7.7% as the pH increased from 4.1 to 10.2. Also, Han *et al.*'s[113] study confirmed that the adsorption of phosphate onto Mg–Al LDH–Alg/PVA beads was not sensitive to pH changes since there was no obvious change in the removal percent of phosphate when the pH increased from 5 to 9.[116] This finding suggested that the fabricated Mg–Al LDH/Alg beads could be applied widely over a wide pH range without a noticeable change in their efficiency. In contrast, pH had a vast impact

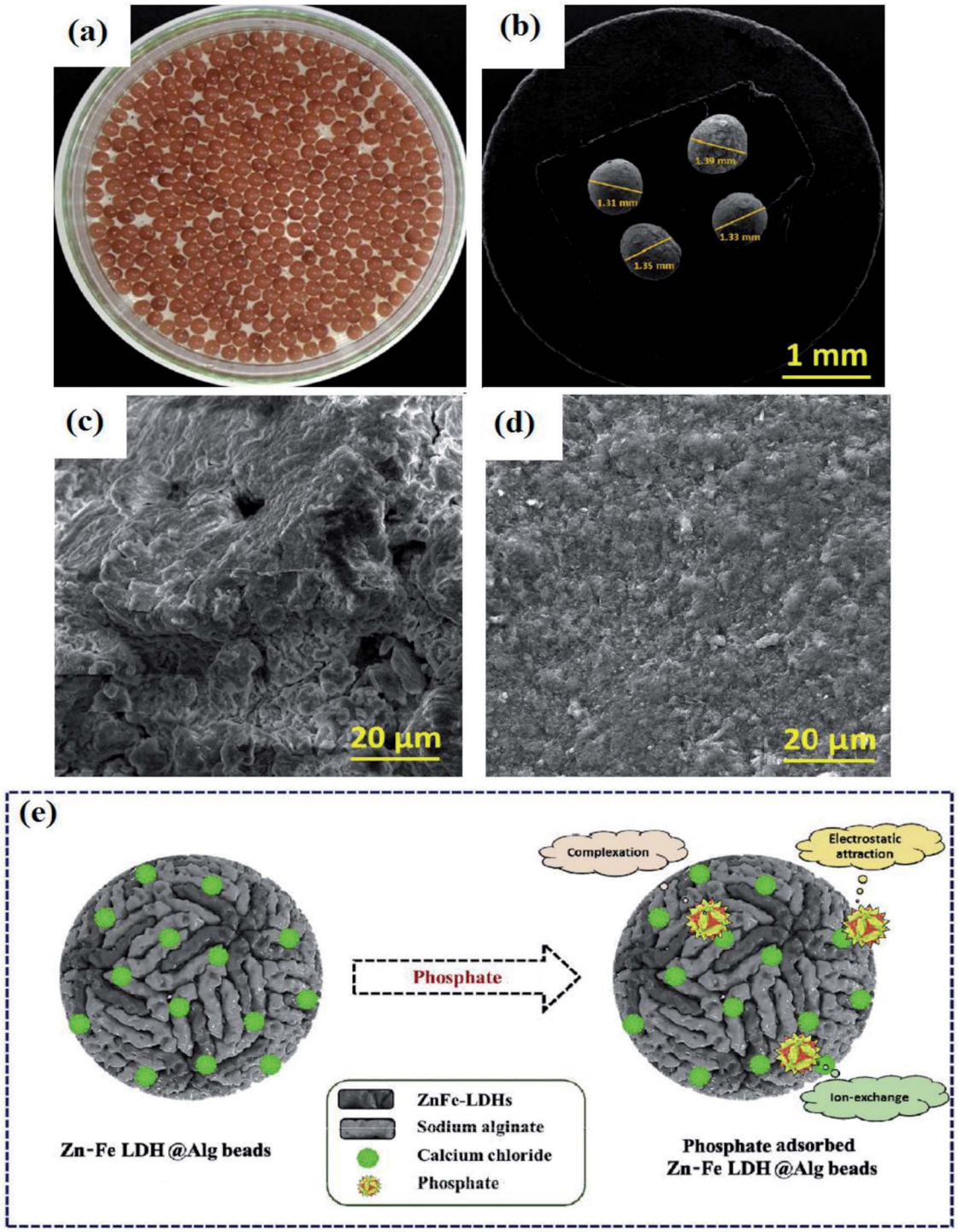

Fig. 10 (a) Digital photo of Zn–Fe LDHs@Alg, (b) SEM of average particle size of Zn–Fe LDHs@Alg, (c) SEM of Zn–Fe LDHs@Alg surface, (d) SEM of Zn–Fe LDHs@Alg after phosphate adsorption, and (e) the proposed adsorption mechanism of phosphate. This figure reproduced from ref. 117 with permission from Elsevier. Copyright (2021).

on phosphate adsorption onto Zn–Fe LDHs@Alg beads. A low adsorption capacity of phosphate in a pH range of 2–3 was recorded, which may be due to the degradation of Zn–Fe LDHs@Alg in a highly acidic medium. While an increase in pH led to an enhancement in the adsorption capacity of Zn–Fe LDHs@Alg towards phosphate ions until it reached its peak at pH 6–7. This may be attributed to the strong electrostatic attraction between HPO_4^{2-} ions and the positively charged surface of Zn–Fe LDHs@Alg beads. Furthermore, it was observed that the adsorption capacity of the beads toward phosphate declined when the pH increased above 7 due to the competition between OH^- and phosphate species. SEM images

(Fig. 10b and c) of Zn–Fe LDHs@Alg revealed that the average porosity of the beads was 1.35 mm. While the pores on the surface of the beads disappeared and the surface became smooth after phosphate adsorption (Fig. 10d). Hence, SEM suggested that the pore-filling mechanism contributed to the phosphate adsorption onto Zn–Fe LDHs@Alg, in addition to an ion-exchange mechanism between phosphate ions and hydroxyl groups on the Zn–Fe LDHs@Alg surface. Besides, there was electrostatic interaction between the beads and phosphate ions as well as surface complexation between the cations on the surface of Zn–Fe LDHs@Alg (*viz.*, Zn^{2+}, Fe^{3+}, and Ca^{2+}) and phosphate (Fig. 10e).[117]

In another attempt, Han *et al.*[113] highlighted the adsorptive removal of phosphate ions onto PVA-modified Mg–Al LDH/Alg beads (Mg–Al LDH–PVA/Alg). The stabilities of both Mg–Al LDH–PVA/Alg and Mg–Al LDH/Alg in different concentrations of phosphate solution (50, 100, 150 and 200 mg L^{-1}) were examined to investigate the effect of PVA on the stability of the beads. The results showed that by increasing the concentration of phosphate from 50 mg L^{-1} to 200 mg L^{-1}, the deformation percentage (Fig. 11) of Mg–Al LDH/Alg increased to reach 100%. In contrast, the deformation percentage of Mg–Al LDH–PVA/Alg was 7.8% which is most likely due to the high tensile strength and flexibility of PVA in water. Hence, the blending of Alg with PVA could improve the strength and durability of hydrogel beads.

In the light of this result, Mg–Al LDH–PVA/Alg beads could be regenerated for many cycles, which renders them a cost-effective adsorbent, agreeing with Idris *et al.*'s[118] study that reported the high reusability of PVA/Alg beads. A recyclability test showed the excellent adsorption performance of PVA/Alg beads after the 7th cycle.

2.4. Carbon materials-modified alginate

Over the last decades, carbon-based materials have been widely applied in wastewater remediation owing to their remarkable advantages, including large surface area, high porosity, flexibility, and outstanding thermal and mechanical stability.[119–122] Therefore, blending Alg with such materials could be a promising solution to boosting its mechanical property and its adsorption aptitude towards the removal of phosphate as well.[123] Among these materials, graphene oxide has attracted immense attention due to its unique features, including large surface area, hydrophilicity, flexibility, and structural tenability.[124,125] In this context, Kumar *et al.*[126] fabricated triazine-functionalized graphene oxide encapsulated into alginate beads (TATGO@Alg) for the adsorptive removal of phosphate. Notably, the modification of GO with TAT provides plenty of $-NH_2$ functional groups, boosting the adsorption efficiency of the beads *via* electrostatic attraction between the protonated $-NH_3^+$ and $-OH_2^+$ and phosphate ions.[127] BET measurements showed that TATGO@Alg composite beads possessed a higher S_{BET} (45.29 m^2 g^{-1}) than pure Alg beads (3.27 m^2 g^{-1}). This result suggested the availability of larger numbers of active sites on the TATGO@Alg surface that increase the adsorption capacity of the beads toward phosphate. As a result, TATGO@Alg exhibited a fascinating q_{max} reaching 58.46 mg g^{-1} under optimal conditions of 0.1 g dosage of TATGO@Alg, 100 mg L^{-1} initial concentration of phosphate, pH 7, and contact time of 30 min. Moreover, TATGO@Alg revealed good selectivity towards phosphate ions in the presence of other competing anions, such as $HCrO_4^-$, F^-, SO_4^{2-}, HCO_3^- and Cl^- ions. The existence of SO_4^{2-} caused a significant hindrance to the adsorption of phosphate ions owing to the high charge density and large ionic size of SO_4^{2-} with respect to its counterparts.[105] The adsorption data were best fitted with Langmuir and Freundlich isotherm models as well as pseudo-second-order and intraparticle diffusion kinetic models. The FTIR spectrum of TATGO@Alg pointed out the appearance of new peaks at 1032 and 560 cm^{-1} after the adsorption of phosphate which may be assigned to the stretching and bending vibrations

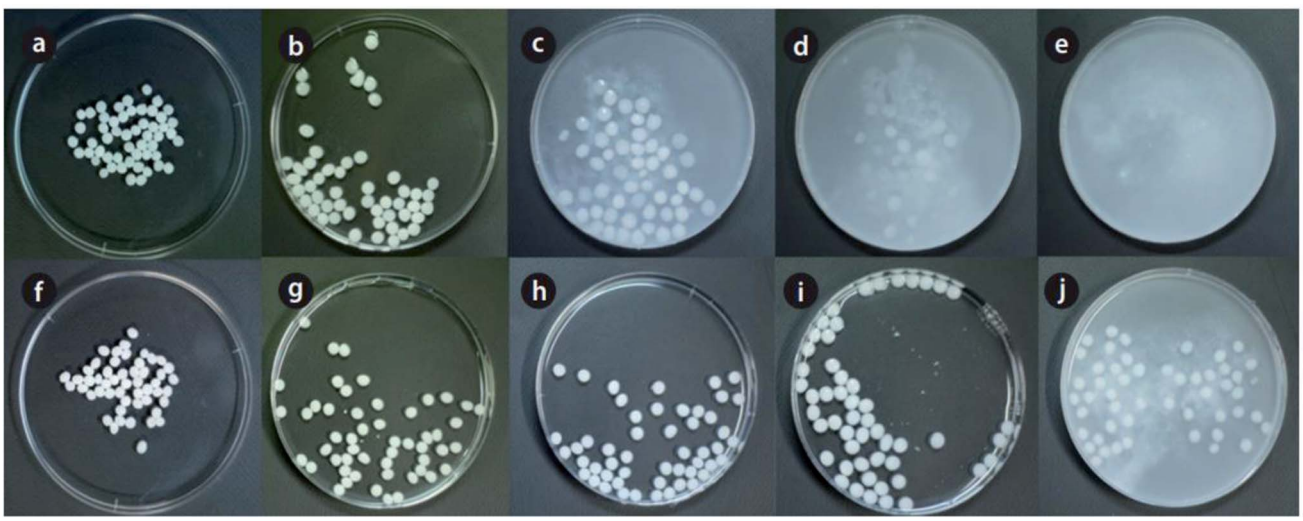

Fig. 11 Deformation of the beads: (a) Mg–Al LDH/Alg beads, (b–e) Mg–Al LDH/Alg beads after phosphate adsorption, (f) before the reaction of LPAB, and (g–j) Mg–Al LDH–PVA/Alg beads after phosphate adsorption. This figure reproduced from ref. 113 with permission from the Korean Society of Environmental Engineers. Copyright (2012).

of the P–O bond, respectively, agreeing with Shan *et al.*'s study.[128] Besides, the presence of a phosphorus peak with an intensity of 9.75% in the EDX spectrum of TATGO@Alg after the adsorption process indicates the excellent uptake of phosphate onto the beads. A recyclability test showed the superb removal efficiency for phosphate (>70%) after the 6th cycle using 0.1 M NaOH as a regenerant, implying the potential applicability and sustainability of TATGO@Alg beads.

In yet another attempt, Shan and his coworkers[128] inspected the adsorption performance of zirconium-crosslinked GO/Alg (Zr–GO/Alg) aerogel beads for removing phosphate. There was excellent synergy between the strong affinity and selectivity of multivalent Zr(IV) towards phosphate adsorption and the perfect mechanical strength of GO.[129,130] Accordingly, Zr–GO/Alg beads exhibited an ultra-adsorption capacity of 189.06 mg g^{-1} at 25 °C using 0.2 g L^{-1} adsorbent dosage. In this case, the pH of the medium was a crucial factor that significantly affected the adsorption behavior of the beads, as depicted in Fig. 12a. It was found that Zr–GO/Alg beads reached a peak adsorptive performance at pH = 2.03 due to the strong electrostatic attraction between the protonated active groups on the Zr–GO/Alg surface ($pH_{pzc} = 7.2$) and $H_2PO_4^-$ species as well as the ligand exchange between $H_2PO_4^-$ and Cl^-. Meanwhile, a continuous decrease in the adsorption capacity occurred when the pH increased from 2 to 7, due to the weaker electrostatic attractions. When pH > 7 the adsorption capacity for phosphate dramatically declined due to the strong electrostatic repulsion between the deprotonated surface of Zr–GO/Alg and phosphate ions as well as OH^- groups that strongly competed with phosphate ions for the binding sites of the beads. For a further understanding of the phosphate adsorption mechanism, XPS spectra of Zr–GO/Alg before and after the adsorption process were estimated. The XPS wide spectrum (Fig. 12b) revealed the peak belonging to P 2p, confirming the adsorption of phosphate onto Zr–GO/Alg beads. Whereas, the Zr 3d-spectrum (Fig. 12c) showed a slight negative shift of Zr $3d_{5/2}$ and Zr $3d_{3/2}$ peaks, implying the

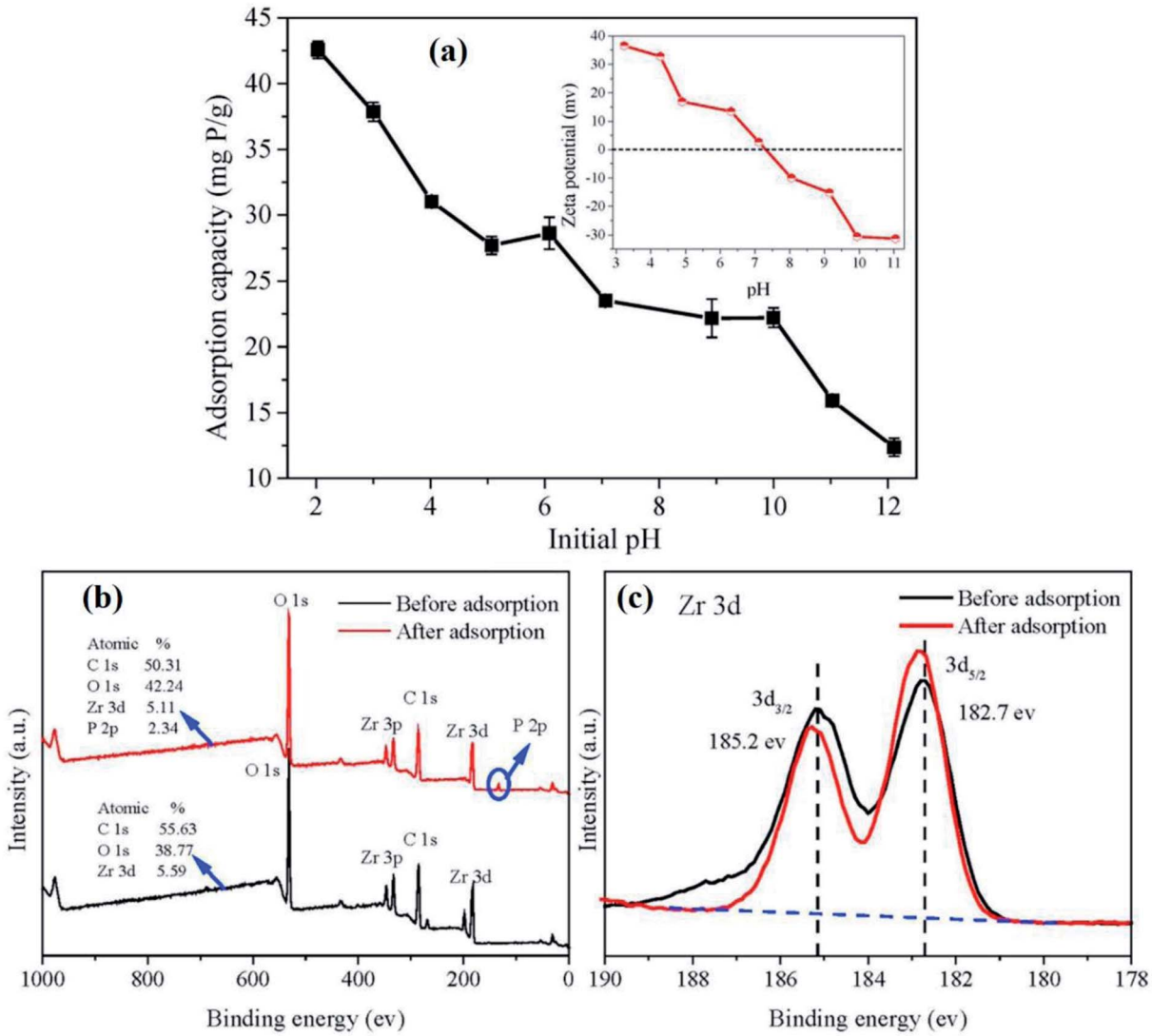

Fig. 12 (a) Effect of pH on the adsorption of phosphate on Zr–GO/Alg aerogel beads and XPS of Zr–GO/Alg before and after the adsorption process. (b) Wide spectra and (c) Zr 3d spectra. This figure reproduced from ref. 128 with permission from Elsevier. Copyright (2019).

domination of the complexation mechanism in the adsorption process.[131] Based on the aforementioned results, the adsorption mechanism of phosphate onto Zr–GO/Alg beads was mainly dominated by electrostatic interactions, complexation, and ligand exchange.

Biochar (BC) is one more carbonaceous material that is derived *via* the thermal treatment of biomass like wood, marine algae, agricultural wastes, rice husk, and wheat straw under a limited oxygen atmosphere.[120,132,133] The structure of BC is distinguished by the presence of abundant oxygen-containing functional groups, high porosity, large surface area, and high mechanical strength.[123] Hence, BC has been established as a green adsorbent and propitious candidate for the cost-effective removal of phosphate. Notably, the adsorption capability of a BC-based adsorbent mainly depends on its natural source and pyrolysis temperature.[134,135] In this regard, Jung *et al.*[136] fabricated BC from three different types of marine macroalgae (*Laminaria japonica*, *Undaria pinnatifida* and *Porphyra tenera*) and studied the impact of pyrolysis temperature on their structural properties and adsorption behavior. *Laminaria japonica*-derived biochar (LBC) exhibited the highest removal efficiency for phosphate (97.02%) owing to its higher Ca/P and Mg/P ratios which increased the ionic strength and boosted the binding strength to phosphate.[137–139] In addition, LBC was fabricated at different temperatures of 200, 400, 600, 800 °C to infer the effect of pyrolysis temperature on its physical properties and adsorption efficiency.[139] It was found that LBC-600 attained the highest removal efficiency, reaching 97.95%. Such a superb removal efficiency may be assigned to the higher S_{BET} of LBC-600 of 79.95 $m^2\ g^{-1}$. Furthermore, the incorporation of LBC-600 into Alg beads (LBC-600@Alg) improved its S_{BET} (242.34 $m^2\ g^{-1}$), suggesting the availability of more adsorption sites to adsorb phosphate. As a result, the q_{max} of LBC-600@Alg towards phosphate ions reached 116.15 mg g^{-1} at 30 °C. It was observed that LBC-600@Alg beads exhibited excellent adsorptive behavior at pH < pH_{pzc} (8.42) owing to the strong electrostatic attraction forces between the protonated binding sites (*i.e.*, hydroxyl and carboxyl) on the beads and the $H_2PO_4^-$

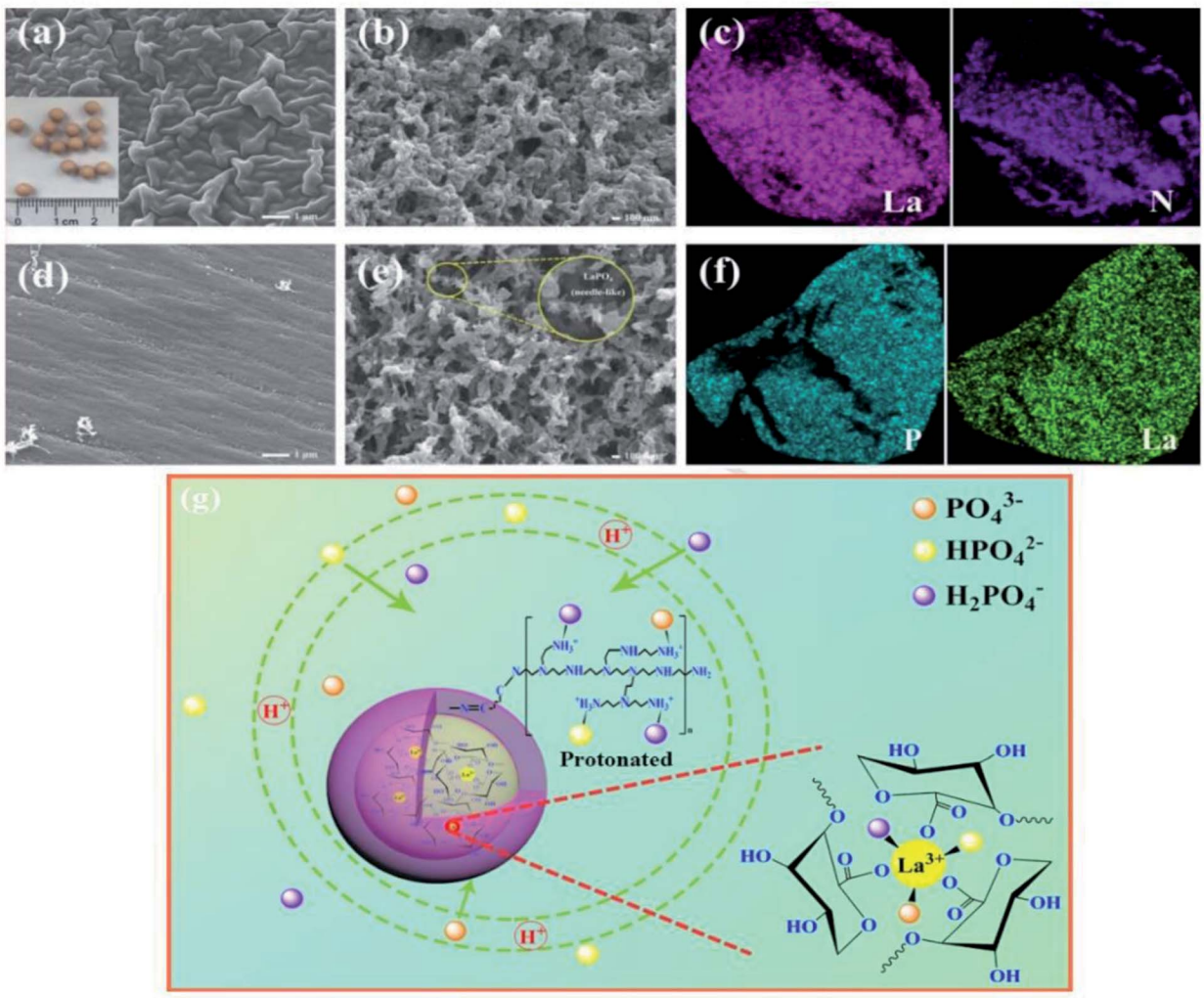

Fig. 13 SEM of Alg–La@PEI beads: (a and b) before adsorption and (d and e) after adsorption. EDX mapping of Alg–La@PEI beads: (c) before adsorption and (f) after adsorption. (g) The plausible adsorption mechanism. This figure reproduced from ref. 141 with permission from Elsevier. Copyright (2020).

species. Whereas at pH > pH_{pzc}, there were robust electrostatic repulsion forces between the deprotonated binding sites of LBC-600@Alg and the PO_4^{3-} anion. Thus, electrostatic interaction dominated the adsorption mechanism of phosphate onto LBC-600@Alg, disagreeing with Cui *et al.*'s study.[123] Phosphate adsorption onto Mg–BC@Alg beads exhibited excellent removal efficiency of 97.1% over a wide pH range from 3 to 10. This behavior indicated that electrostatic interaction had a negligible effect on the adsorption process. It was hypothesized that phosphate ions adsorbed onto Mg–BC@Alg *via* the complexation mechanism between phosphate ions and Ca^{2+}, Mg^{2+} and Al^{3+} played a significant role in the adsorption process. In addition, ligand exchange occurred between $Mg(OH)_2$ onto the Mg–BC@Alg surface and $H_2PO_4^-$ as in the following equation:[140]

$$Mg(OH)_2 + 2H_2PO_4^- \rightarrow Mg(H_2PO_4)_2 + 2OH^- \quad (5)$$

2.5. Multivalent metal-based alginate

To improve the adsorption capability and mechanical strength of Alg, several studies have deemed the incorporation of multivalent metals into the Alg matrix to be an effective modification technique. From this perspective, Zhao *et al.*[141] successfully designed Alg–La@polyethyleneimine beads (Alg–La@PEI) as an eco-friendly and cost-effective adsorbent for removing phosphate from aqueous media. SEM images (Fig. 13a and b) showed that the size of the fabricated Alg–La@PEI was around 4 mm. While SEM images (Fig. 13d and e) verified the adsorption of phosphate onto the beads since the surface of the beads became smoother. EDX spectra of Alg–La@PEI (Fig. 13c and f) revealed the presence of phosphorus, also confirming the phosphate adsorption. Indeed, the strong affinity between La^{3+} and phosphate exhibited great participation in the enhancement of the phosphate uptake onto Alg–La@PEI at which it facilitated the formation of $LaPO_4$ precipitate (KSP = 10^{-25}).[142,143] In addition there was Lewis acid–base interaction between La^{3+} and phosphate and electrostatic interaction between the abundant $-NH_2$ on the Alg–La@PEI surface and phosphate ions (Fig. 13g).[144,145] This proposed mechanism was consistent with Luo *et al.*'s[146] study that proposed electrostatic attraction, ligand exchange, and inner-sphere complexation as plausible adsorption mechanisms for the adsorption of phosphate onto PEG-modified PNIPAM/Alg–Zr beads.

The adsorption selectivity of SA–La@PEI towards phosphate was tested in the presence of interfering ions such as NO_3^-, HCO_3^-, SO_4^{2-}, and Cl^-, showing good selectivity towards phosphate with a slight decrease in the adsorption capacity in the presence of NO_3^-, SO_4^{2-}, and Cl^- ions. However, there was an observable decline in the adsorption capacity in the presence of HCO_3^- that may be related to the basic nature of bicarbonate that raised the pH of the medium and altered the surface potential of the adsorbent.[147] Moreover, SA–La@PEI beads showed a promising removal efficiency of up to 78% after 5

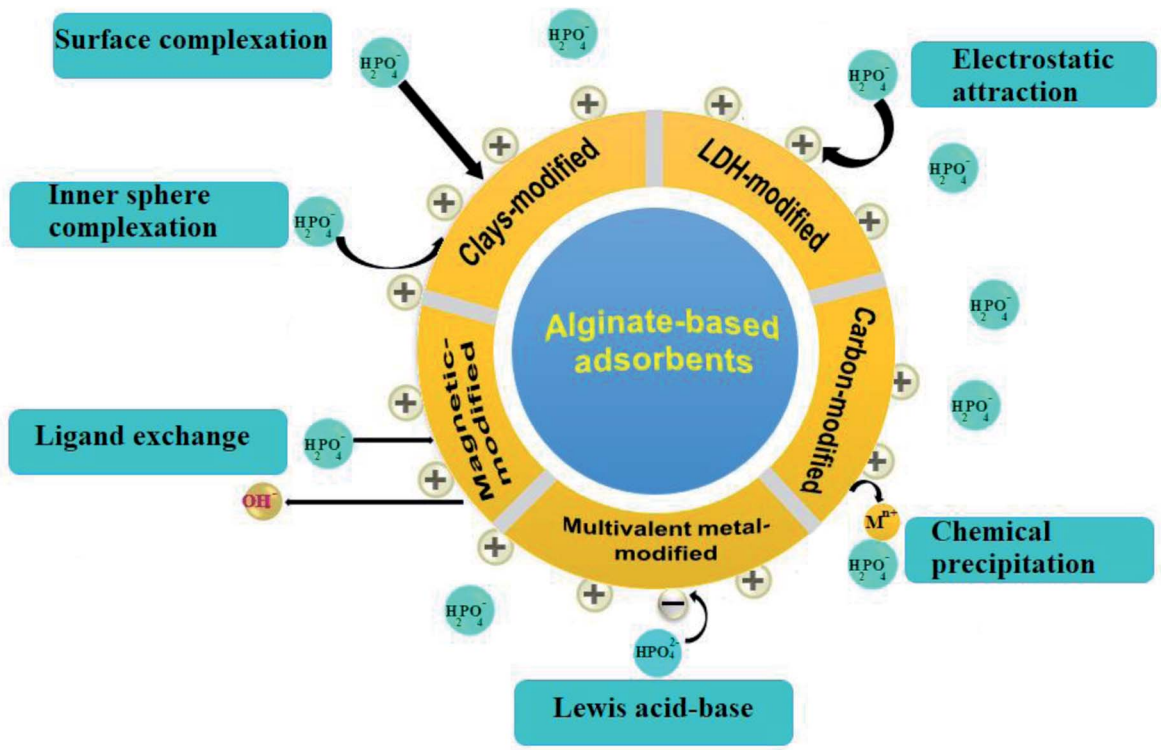

Fig. 14 The main modifications for alginate-based adsorbents and the most common adsorption mechanisms of phosphate ions by alginate-based adsorbents.

Table 1 Adsorption conditions, adsorption capacities, kinetics, and isotherms of phosphate adsorption by various alginate-based adsorbents

Modification strategy	Adsorbent	S_{BET} m^2 g^{-1}	q_{max} mg g^{-1}	pH	Eq. time (min)	Kinetics model	Isotherm	Adsorption mechanism	Ref.
Clays-modified alginate	Alg–MgO@BT beads	59.5	70.5	3–10	300–1200	Pseudo-2nd order	Langmuir	Mg–P complexation formation Electrostatic attraction Ligand exchange	90
	Zr@AlgKN beads (hydro)	78.9	37.2	2–7	30	Pseudo-2nd order	Freundlich	Electrostatic attraction Surface complexation Ion exchange	85
	MtIAlg beads	—	48.7	2–10	30	Pseudo-2nd order	Langmuir	Ligand exchange Surface complexation Electrostatic attraction	82
	La/PVA/Alg/Pal beads	5.8	33.2	3–6	720	Pseudo-2nd order	Freundlich	Electrostatic attraction and ligand exchange (acidic condition) Lewis acid–base interaction (alkaline condition)	95
	Al–NaBT–Alg beads	17.0	15.8	3	360–2880	Pseudo-2nd order	Sips	Ligand exchange Anion exchange Electrostatic attraction	74
	NH–Alg–ZrBT beads	53.8	63.6	3–9	600–3000	Pseudo-2nd order	Langmuir	Electrostatic attraction Inner-sphere complexation Ligand exchange	93
	$MgCl_2$–BT@Alg microspheres	46.2	46.6	3–10	1440	Pseudo-2nd order	Freundlich	Chemical precipitation Ligand exchange	123
	Talc/Alg/La beads	—	16.4	4	21 600	Pseudo-2nd order	Langmuir	Electrostatic attraction and ligand exchange (acidic condition) Complexation (alkaline condition)	152
Magnetic materials-modified alginate	Fe_3O_4/PAM/SA–Zr beads	24.7	42.2	2	1800	Pseudo-2nd order	Freundlich	Electrostatic attraction (physisorption) Ligand exchange (chemisorption)	102
	La–$MgFe_2O_4$/BC@Alg beads	158.8	26.8	5–8	800–950	Pseudo-2nd order	Langmuir	Electrostatic attraction Inner-sphere complexation Ligand exchange	100
	Alg/α-FeOOH composite	—	36.0	4–10	15 840	—	Freundlich	Electrostatic attraction	94
	AFMAlg beads (hydro)	79.4	30.1	5	30	Pseudo-2nd order	Freundlich	Electrostatic attraction Surface complexation	101
	AFMAlg beads (*in situ*)	65.0	25.1						
Layered double hydroxides-modified alginate	ZnFe-LDHs@Alg beads	1.1	94.6	4–7	60	Pseudo-2nd order	Freundlich	Electrostatic attraction Surface complexation Ion exchange	117
	LDH–Alg beads	—	1.0	4.9–8.9	720	Pseudo-2nd order	Freundlich	Electrostatic attraction Anion exchange Anion intercalation	114
	Mg–Al LDH–Alg/PVA beads	—	1.9	5.7	480	Pseudo-2nd order	Freundlich/Langmuir	—	116
	LDH–PVA/Alg beads	—	0.4	4.9	720	—	Freundlich	Electrostatic attraction Anion exchange Anion intercalation	113
Carbon materials-modified alginate	Zr–GO/Alg beads	—	189.1	2.03	720	Pseudo-2nd order	Freundlich	Ligand exchange Electrostatic attraction	128

Table 1 (*Contd.*)

Modification strategy	Adsorbent	S_{BET} m^2 g^{-1}	q_{max} mg g^{-1}	pH	Eq. time (min)	Kinetics model	Isotherm	Adsorption mechanism	Ref.
								Chemical precipitation	
	LBC–Alg beads	242.3	157.7	6	1440	Pseudo-2nd order	Langmuir and Freundlich	—	136
	EMB–Alg beads	177.5	169.9	4	1440	Pseudo-2nd order	Sips	—	153
	TATGO@Alg composite beads	45.3	58.5	7	30	Pseudo-2nd order	Freundlich	Electrostatic attraction	126
	AC@Alg beads	—	133.3	10	20	Pseudo-2nd order	Langmuir	—	154
	AC@Alg beads	—	0.34	4	45	—	Freundlich	—	155
Multivalent metals-based alginate	Alg–La@PEI beads	—	121.2	3	402	Pseudo-2nd order	Freundlich	Electrostatic attraction Chemical precipitation	141
	Fe–CS–Alg beads	—	84.7	3–6	40	Pseudo-2nd order	Freundlich	Electrostatic attraction Surface complexation Ion exchange	156
	Alg/$FeCl_3$ capsules	—	—	4–10	2880	—	Freundlich	Electrostatic attraction Chemical precipitation	157
	Zr(IV)/red mud@Zn–alginate beads	—	13.6	8	120	Pseudo-2nd order	Langmuir	—	158
	nZrO_2–Al–Alg beads	—	173.0	7	35	Pseudo-2nd order	Freundlich	—	159
	LaC@Alg beads	22.7	42.5	5	120	—	—	Chemical precipitation	160
	$CaCO_3$–Alg beads	—	0.12	10	150	Pseudo-2nd order	Freundlich	—	161
	Alg–Ca–Ce	—	41.4	2	240	Pseudo-2nd order	Langmuir	Electrostatic attraction Lewis acid–base interaction	162
	PEG-modified PNIPAM/Alg–Zr bead	34.1	47.4	2	1800	Pseudo-2nd order	Langmuir	Electrostatic attraction Inner-sphere complexation Ligand exchange	163
	(PVA–SA–LH) hydrogel beads	—	7.9	4	1440	Pseudo-2nd order	Freundlich	Electrostatic attraction Lewis acid–base interaction	164
	Alg–*n*ZVI beads	—	—	12	60	—	—	—	165

cycles, implying excellent mechanical stability of the fabricated beads.

In another study, Luo and his coworkers[146] fabricated interpenetrated Zr–Alg beads decorated with polyethylene glycol beads (PEG-modified PNIPAM/Alg–Zr), merging the excellent adsorption capability with good mechanical and chemical stability. In detail, PEG-modified PNIPAM/Alg–Zr beads exhibited a superb adsorption capability provided by Zr^{4+} ions that have a strong affinity towards phosphate.[129] Good mechanical stability is accomplished by the formation of interpenetration networks. In addition, the macro-porosity formed by PEG during the polymerization facilitated the transfer of ions from the bulk solutions to the active adsorptive sites, boosting the adsorption efficiency. More importantly, PEG-modified PNIPAM/Alg–Zr beads showed a thermo-sensitive behavior which affected their adsorption performance and the swelling ratio of the beads.[148] At low temperatures, the beads became a swollen gel, facilitating the diffusion of phosphate into their matrices, and thus increasing their adsorption capacity. On the other hand, the beads shrank owing to the hydrophobicity of PNIPAM at temperatures higher than the vapor phase transition temperature, so the adsorption capability of the beads declined. As a result, the adsorption capacity of PEG-modified PNIPAM/Alg–Zr beads decreased from 36.90 to 34.00 mg g^{-1} when the temperature was raised from 25 to 65 °C. PEG-modified PNIPAM/Alg–Zr beads reached 99% desorption efficiency in 40 min at 55 °C using 0.2 M NaOH. This excellent result may be anticipated from the compactness of the adsorptive sites after the shrinkage of the beads, so phosphate ions become weakly bound to the active sites, and thus easily desorbed.[149] It was found that the higher adsorption capacity of phosphate was 36.06 mg g^{-1} at pH 2 since the predominant species were $H_2PO_4^-$ and H_3PO_4.[150] So, electrostatic attraction occurred between $H_2PO_4^-$ and the positively charged PEG-modified PNIPAM/Alg–Zr surface ($pH_{pzc} = 3.8$). In contrast, the adsorption aptitude of phosphate onto talc/Alg/La beads was almost the same over a wide pH range. Talc/Alg/La demonstrated a superior phosphate removal efficacy of up to 85% at pH values of 4, 7, and 10. Moreover, talc/Alg/La beads retained their physical and chemical properties in both acidic and alkaline conditions, thus verifying their excellent chemical and mechanical stability and applicability for wastewater treatment.[151]

3. Summary, discussion and future recommendations

There are several reported works on the removal of phosphate using different alginate-based adsorbents, including clay-modified, magnetic-modified, carbon-modified, layered double hydroxide-modified and multivalent-modified alginate adsorbents. The carbon-modified alginate adsorbents showed the highest performance while magnetic-modified ones provide the easiest separation route. Clay-modified and multivalent metal-modified alginate adsorbents show reasonable adsorption performance; however, most layered double hydroxide-modified alginate adsorbents demonstrated a low adsorption performance. The removal process of phosphate by all alginate-modified adsorbents revealed an almost pseudo-2nd-order kinetic model. The main modifications of alginate adsorbents and the most common adsorption mechanisms are illustrated in Fig. 14.

Moreover, it was found that a variation in the optimum pH to adsorb phosphate ions onto alginate-based adsorbents may be attributed to the polyprotic nature of phosphate, resulting in electrostatic interaction/repulsion forces between phosphate and the adsorbents. Furthermore, in some cases, phosphate adsorption was not sensitive to pH change, which is most likely due to the domination of other adsorption mechanisms, such as ion exchange, complexation, precipitation and Lewis acid–base interaction. Hence, one or more of these mechanisms could surpass electrostatic interaction, hindering the effect of pH on the adsorption efficacy. Moreover, studying coexisting ions on the adsorption efficiency of phosphate implied that SO_4^{2-} caused a significant hindrance to the adsorption process owing to its high charge density and large ionic size. Nonetheless, some studies confirmed that alginate-based adsorbents still had a high selectivity towards phosphate ions in the presence of diverse interfering ions. Moreover, based on concrete results, the incorporation of layered double hydroxides, clays and carbon materials into the alginate matrix significantly improved the adsorption performance of the developed alginate adsorbents toward phosphate ions.

The experimental conditions of the adsorption of phosphate by various alginate-based adsorbents in addition to the adsorption capacities, kinetics, and isotherms are summarized in Table 1.

This review evinces the viability of recent ways of developing the adsorbability of alginate toward phosphate ions. However, we hold to the notion that the aforementioned modified forms of alginate still suffer from flaws; most of them need to be shaped as beads, hydrogels, or membranes to provide perfect separation, even though this decreases the surface area of the adsorbents. In addition, there is a probability that these fine materials can leach from the pores of the shaped alginate forms into water, causing another type of contamination. Furthermore, we could not neglect the economic aspect since most of the materials used to modify alginate are costly.

Therefore, based on this in-depth study, we recommend some serious points that should be taken into consideration in future investigations:

✓ Sustainable studies to fabricate efficient alginate-based adsorbents with promising adsorbability and selectivity toward phosphate ions.

✓ Improving the durability of the shaped alginate forms to avoid leaching of the incorporated materials.

✓ From the economic aspect, scalable fabrication of alginate-based adsorbents at an affordable cost is an important issue.

✓ Developing a magnetic-based alginate to provide practical, perfect, and easy separation which will increase the reusability of the adsorbents is another case from the economical point of view.

Finally, it is crucial to mention the lack of column experiments in the majority of the published research papers, though fixed-bed studies are essential for real applications from an industrial perspective.

4. Conclusion

In general, the removal of phosphate ions from wastewater is a critical topic, although it has not been discussed adequately in recent literature. Meanwhile, alginate has drawn a huge amount of consideration as a future wave of plentiful resources that should be exploited. Consequently, the present review has reported the adsorptive removal of noxious phosphate ions from wastewater by alginate-based adsorbents, focusing on advanced methods to foster the physical properties and the adsorption behavior of alginate. Notably, the optimum adsorption conditions of phosphate ions onto the developed alginate forms were well explained. More importantly, the adsorption mechanisms of phosphate ions onto the most popular alginate-based adsorbents were elucidated. Moreover, based on these concrete results, the incorporation of layered double hydroxides and carbon materials into the alginate matrix significantly improved the adsorption capacity of the developed alginate adsorbents toward phosphate ions.

Conflicts of interest

There are no conflicts to declare.

References

1 M. Hosny, A. S. Eltaweil, M. Mostafa, Y. A. El-Badry, E. E. Hussein, A. M. Omer and M. Fawzy, *ACS Omega*, 2022, **7**(3), 3121–3133.

2 M. Hosny, M. Fawzy, Y. A. El-Badry, E. E. Hussein and A. S. Eltaweil, *J. Saudi Chem. Soc.*, 2022, 101419, DOI: 10.1016/j.jscs.2022.101419.

3 A. M. Omer, A. El-Monaem, M. Eman, G. M. El-Subruiti, A. El-Latif, M. Mona and A. S. Eltaweil, *Sci. Rep.*, 2021, **11**, 1–14.

4 H. A. Elbadawy, W. A. Sadik, A. F. Elhusseiny and S. M. Hussein, *Process Saf. Environ. Prot.*, 2021, **148**, 1191–1206.

5 H. A. Elbadawy, A. H. Abdel-Salam and T. E. Khalil, *Microchem. J.*, 2021, **165**, 106097.

6 H. Wang, X. Xu, Z. Ren and B. Gao, *RSC Adv.*, 2016, **6**, 47237–47248.

7 A. S. Eltaweil, E. M. A. El-Monaem, M. S. Mohy-Eldin and A. M. Omer, *Sci. Rep.*, 2021, **11**, 1–15.

8 N. El-Maghrabi, O. M. El-Borady, M. Hosny and M. Fawzy, *ACS Omega*, 2021, **6**(50), 34954–34966.

9 A. El-Monaem, M. Eman, A. M. Omer, G. M. El-Subruiti, M. S. Mohy-Eldin and A. S. Eltaweil, *Biomass Convers. Biorefin.*, 2022, 1–13, DOI: 10.1007/s13399-022-02362-y.

10 M. Hosny, M. Fawzy, E. M. El-Fakharany, A. M. Omer, E. M. A. El-Monaem, R. E. Khalifa and A. S. Eltaweil, *J. Environ. Chem. Eng.*, 2022, **10**, 106806.

11 A. S. Eltaweil, M. Fawzy, M. Hosny, E. M. Abd El-Monaem, T. M. Tamer and A. M. Omer, *Arabian J. Chem.*, 2022, **15**, 103517.

12 A. S. Eltaweil, A. M. Omer, H. G. El-Aqapa, N. M. Gaber, N. F. Attia, G. M. El-Subruiti, M. S. Mohy-Eldin and E. M. Abd El-Monaem, *Carbohydr. Polym.*, 2021, 118671.

13 M. H. Mahaninia and L. D. Wilson, *J. Colloid Interface Sci.*, 2017, **485**, 201–212.

14 H. Shen, Z. Wang, A. Zhou, J. Chen, M. Hu, X. Dong and Q. Xia, *RSC Adv.*, 2015, **5**, 22080–22090.

15 P. Karthikeyan and S. Meenakshi, *J. Environ. Chem. Eng.*, 2020, **8**, 103530.

16 Y. Zhang, B. Pan, C. Shan and X. Gao, *Environ. Sci. Technol.*, 2016, **50**, 1447–1454.

17 X. Xu, B.-Y. Gao, X. Tan, Q.-Y. Yue, Q.-Q. Zhong and Q. Li, *Carbohydr. Polym.*, 2011, **84**, 1054–1060.

18 H. A. T. Banu, P. Karthikeyan, S. Vigneshwaran and S. Meenakshi, *Int. J. Biol. Macromol.*, 2020, **154**, 188–197.

19 S. P. Boeykens, M. N. Piol, L. S. Legal, A. B. Saralegui and C. Vázquez, *J. Environ. Manage.*, 2017, **203**, 888–895.

20 G. Maier, R. J. Nimmo-Smith, G. A. Glegg, A. D. Tappin and P. J. Worsfold, *Aquat. Conserv.: Mar. Freshw. Ecosyst.*, 2009, **19**, 43–56.

21 F. Edition, *WHO Chron.*, 2011, **38**, 104–108.

22 S. Gu, X. Kang, L. Wang, E. Lichtfouse and C. Wang, *Environ. Chem. Lett.*, 2019, **17**, 629–654.

23 G. Tokazhanov, E. Ramazanova, S. Hamid, S. Bae and W. Lee, *Chem. Eng. J.*, 2020, **384**, 123252.

24 Y. Li, F. Fu, W. Cai and B. Tang, *Powder Technol.*, 2019, **345**, 786–795.

25 A. M. Abdelfatah, M. Fawzy, A. S. Eltaweil and M. E. El-Khouly, *ACS Omega*, 2021, **6**, 25397–25411.

26 F. D. Belkada, O. Kitous, N. Drouiche, S. Aoudj, O. Bouchelaghem, N. Abdi, H. Grib and N. Mameri, *Sep. Purif. Technol.*, 2018, **204**, 108–115.

27 P. Karthikeyan, H. A. T. Banu and S. Meenakshi, *Int. J. Biol. Macromol.*, 2019, **124**, 492–504.

28 H. He, Y. Huang, M. Yan, Y. Xie and Y. Li, *Colloids Surf., A*, 2020, **584**, 123973.

29 M. Diab, N. F. Attia, A. Attia and M. El-Shahat, *Synth. Met.*, 2020, **265**, 116411.

30 C. Liu, R.-N. Jin, X.-k. Ouyang and Y.-G. Wang, *Appl. Surf. Sci.*, 2017, **408**, 77–87.

31 T. Tamer, W. Abou-Taleb, G. Roston, M. Mohyeldin, A. Omer, R. Khalifa and A. Hafez, *Environ. Nanotechnol. Monit. Manag.*, 2018, **10**, 112–121.

32 A. S. Eltaweil, E. M. Abd El-Monaem, G. M. El-Subruiti, M. M. Abd El-Latif and A. M. Omer, *RSC Adv.*, 2020, **10**, 19008–19019.

33 X. Lv, J. Xu, G. Jiang, J. Tang and X. Xu, *J. Colloid Interface Sci.*, 2012, **369**, 460–469.

34 Y. An, H. Zheng, Z. Yu, Y. Sun, Y. Wang, C. Zhao and W. Ding, *J. Hazard. Mater.*, 2020, **381**, 120971.

35 A. Sharmin, M. A. Hai, M. M. Hossain, M. M. Rahman, M. B. Billah, S. Islam, M. Jakariya and G. C. Smith, *Groundw. Sustain. Dev.*, 2020, **10**, 100348.

36 B. Wang, X. Hu, D. Zhou, H. Zhang, R. Chen, W. Guo, H. Wang, W. Zhang, Z. Hong and W. Lyu, *J. Cleaner Prod.*, 2021, 126878.
37 A. M. Abdelfatah, M. Fawzy, A. S. Eltaweil and M. E. El-Khouly, *ACS Omega*, 2021, **6**(39), 25397–25411.
38 A. M. Abdelfatah, M. Fawzy, M. E. El-Khouly and A. S. Eltaweil, *J. Saudi Chem. Soc.*, 2021, **25**, 101365.
39 K.-W. Jung, S. Y. Lee, J.-W. Choi and Y. J. Lee, *Chem. Eng. J.*, 2019, **369**, 529–541.
40 S. Kilpimaa, H. Runtti, T. Kangas, U. Lassi and T. Kuokkanen, *Chem. Eng. Res. Des.*, 2014, **92**, 1923–1933.
41 J.-h. Li, G.-h. Lv, W.-b. Bai, Q. Liu, Y.-c. Zhang and J.-q. Song, *Desalin. Water Treat.*, 2016, **57**, 4681–4693.
42 W. Huang, X. Yu, J. Tang, Y. Zhu, Y. Zhang and D. Li, *Microporous Mesoporous Mater.*, 2015, **217**, 225–232.
43 K. Karageorgiou, M. Paschalis and G. N. Anastassakis, *J. Hazard. Mater.*, 2007, **139**, 447–452.
44 J. Lalley, C. Han, G. R. Mohan, D. D. Dionysiou, T. F. Speth, J. Garland and M. N. Nadagouda, *Environ. Sci.: Water Res. Technol.*, 2015, **1**, 96–107.
45 W. Jiang, J. Lv, L. Luo, K. Yang, Y. Lin, F. Hu, J. Zhang and S. Zhang, *J. Hazard. Mater.*, 2013, **262**, 55–63.
46 T. P. Kumar, T. R. Mandlimath, P. Sangeetha, S. Revathi and S. A. Kumar, *Environ. Chem. Lett.*, 2018, **16**, 389–400.
47 E. Peleka and E. Deliyanni, *Desalination*, 2009, **245**, 357–371.
48 S. Lu, S. Bai, L. Zhu and H. Shan, *J. Hazard. Mater.*, 2009, **161**, 95–101.
49 S. N. Milmile, J. V. Pande, S. Karmakar, A. Bansiwal, T. Chakrabarti and R. B. Biniwale, *Desalination*, 2011, **276**, 38–44.
50 A. Keränen, T. Leiviskä, O. Hormi and J. Tanskanen, *J. Environ. Manage.*, 2015, **147**, 46–54.
51 E. M. Abd El-Monaem, A. S. Eltaweil, H. M. Elshishini, M. Hosny, M. M. Abou Alsoaud, N. F. Attia, G. M. El-Subruiti and A. M. Omer, *Arabian J. Chem.*, 2022, 103743.
52 T. Baran and M. Nasrollahzadeh, *Int. J. Biol. Macromol.*, 2020, **148**, 565–573.
53 S. Iravani and R. S. Varma, *Green Chem.*, 2020, **22**, 612–636.
54 N. Oladoja, R. Adelagun, A. Ahmad, E. Unuabonah and H. Bello, *Colloids Surf., B*, 2014, **117**, 51–59.
55 C. Xu, M. Nasrollahzadeh, M. Sajjadi, M. Maham, R. Luque and A. R. Puente-Santiago, *Renewable Sustainable Energy Rev.*, 2019, **112**, 195–252.
56 A. S. Eltaweil, A. M. Omer, H. G. El-Aqapa, N. M. Gaber, N. F. Attia, G. M. El-Subruiti, M. S. Mohy-Eldin and E. M. Abd El-Monaem, *Carbohydr. Polym.*, 2021, **274**, 118671.
57 M. M. Eldin, A. Omer, E. Soliman and E. Hassan, *Desalin. Water Treat.*, 2013, **51**, 3196–3206.
58 T. Song, W. Tian, J. Zhao, K. Qiao, M. Zou and M. Chu, *J. Taiwan Inst. Chem. Eng.*, 2021, **125**, 168–175.
59 W. Jia, R. Fan, J. Zhang, Z. Geng, P. Li, J. Sun, S. Gai, K. Zhu, X. Jiang and Y. Yang, *Food Chem.*, 2022, 132054.
60 Y. Wei, L. Wang and J. Wang, *Colloids Surf., A*, 2021, 128161.
61 M. Nishida, S. Matsuo, K. Yamanari, M. Iwahara and K. Kusakabe, *Processes*, 2021, **9**, 1657.
62 H. Gomaa, A. Sayed, M. Mahross, M. Abdel-Hakim, I. M. Othman, J. Li and S. M. El-Bahy, *Microporous Mesoporous Mater.*, 2022, **330**, 111578.
63 A. M. Omer, R. Dey, A. S. Eltaweil, E. M. Abd El-Monaem and Z. M. Ziora, *Arabian J. Chem.*, 2022, **15**, 103543.
64 A. S. Eltaweil, I. M. Mamdouh, E. M. Abd El-Monaem and G. M. El-Subruiti, *ACS Omega*, 2021, **6**, 23528–23541.
65 A. M. Omer, M. S. Ahmed, G. M. El-Subruiti, R. E. Khalifa and A. S. Eltaweil, *Pharmaceutics*, 2021, **13**, 338.
66 S. H. Rashedy, M. S. Abd El Hafez, M. A. Dar, J. Cotas and L. Pereira, *Appl. Sci.*, 2021, **11**, 6290.
67 M. Szekalska, A. Puciłowska, E. Szymańska, P. Ciosek and K. Winnicka, *Int. J. Polym. Sci.*, 2016, **2016**, 1–18.
68 R. A. Raus, W. M. F. W. Nawawi and R. R. Nasaruddin, *Asian J. Pharm. Sci.*, 2021, **16**, 280–306.
69 J. P. Hallett and T. Welton, *Chem. Rev.*, 2011, **111**, 3508–3576.
70 M. Younes, P. Aggett, F. Aguilar, R. Crebelli, M. Filipič, M. J. Frutos, P. Galtier, D. Gott and U. Gundert-Remy, *EFSA J.*, 2017, **15**, 05049.
71 F. N. Sorasitthiyanukarn, C. Muangnoi, P. Rojsitthisak and P. Rojsitthisak, *Carbohydr. Polym.*, 2021, **256**, 117426.
72 X. Jin, H. Jiang, F. Qiao, W. Huang, X. Bao, Z. Wang and Q. Hu, *J. Appl. Polym. Sci.*, 2021, **138**, 49697.
73 S. Mallakpour and V. Behranvand, *Int. J. Biol. Macromol.*, 2021, **180**, 28–35.
74 X. Xu, B. Wang, H. Tang, Z. Jin, Y. Mao and T. Huang, *J. Environ. Manage.*, 2020, **260**, 110130.
75 K. Y. Lee and D. J. Mooney, *Prog. Polym. Sci.*, 2012, **37**, 106–126.
76 T. Senturk Parreidt, K. Müller and M. Schmid, *Foods*, 2018, **7**, 170.
77 M. Mohy Eldin, A. Omer, M. Wassel, T. Tamer, M. Abd Elmonem and S. Ibrahim, *Int. J. Pharm. Pharm. Sci.*, 2015, **7**, 331–337.
78 F. Aziz, M. El Achaby, A. Lissaneddine, K. Aziz, N. Ouazzani, R. Mamouni and L. Mandi, *Saudi J. Biol. Sci.*, 2020, **27**, 2499–2508.
79 M. S. Shamsudin, S. F. Azha, L. Sellaoui, M. Badawi, A. Bonilla-Petriciolet and S. Ismail, *Chem. Eng. J.*, 2022, **428**, 131929.
80 H. Kaygusuz and F. Erim, *React. Funct. Polym.*, 2013, **73**, 1420–1425.
81 W.-J. Dai, P. Wu, D. Liu, J. Hu, Y. Cao, T.-Z. Liu, C. P. Okoli, B. Wang and L. Li, *Chemosphere*, 2020, **251**, 126074.
82 T. K. Das, Q. Scott and A. N. Bezbaruah, *Chemosphere*, 2021, **281**, 130837.
83 P. Karthikeyan and S. Meenakshi, *Int. J. Biol. Macromol.*, 2021, **168**, 750–759.
84 L. Deng and Z. Shi, *J. Alloys Compd.*, 2015, **637**, 188–196.
85 I. A. Kumar and N. Viswanathan, *Arabian J. Chem.*, 2020, **13**, 4111–4125.
86 Y. Abdellaoui, H. Abou Oualid, A. Hsini, B. El Ibrahimi, M. Laabd, M. El Ouardi, G. Giácoman-Vallejos and P. Gamero-Melo, *Chem. Eng. J.*, 2021, **404**, 126600.
87 A. A. Aryee, F. M. Mpatani, X. Zhang, A. N. Kani, E. Dovi, R. Han, Z. Li and L. Qu, *J. Cleaner Prod.*, 2020, **268**, 122191.

88 Q. Song, S. Huang, L. Xu, N. Wang, Z. Hu, X. Luo and Z. Zheng, *Sci. Total Environ.*, 2020, **723**, 137838.
89 J. Lin, B. Jiang and Y. Zhan, *J. Environ. Manage.*, 2018, **217**, 183–195.
90 H. Xi, H. Jiang, D. Zhao, A. H. Zhang, B. Fan, Y. Yang and J. Zhang, *J. Cleaner Prod.*, 2021, 127773.
91 L. Deng, D. Zhang, Z. Kong, L. He, Q. Guan and P. Ning, *Ind. Eng. Chem. Res.*, 2020, **59**, 14578–14586.
92 H. Huan, H. Jile, Y. Tang, X. Li, Z. Yi, X. Gao, X. Chen, J. Chen and P. Wu, *Micromachines*, 2020, **11**, 309.
93 H. Xi, Q. Li, Y. Yang, J. Zhang, F. Guo, X. Wang, S. Xu and S. Ruan, *Appl. Clay Sci.*, 2021, **201**, 105919.
94 H. Siwek, A. Bartkowiak and M. Włodarczyk, *Water*, 2019, **11**, 633.
95 B. Wang, X. Hu, D. Zhou, H. Zhang, R. Chen, W. Guo, H. Wang, W. Zhang, Z. Hong and W. Lyu, *J. Cleaner Prod.*, 2021, **298**, 126878.
96 K.-W. Jung, S. Lee and Y. J. Lee, *Bioresour. Technol.*, 2017, **245**, 751–759.
97 C. Wu, J. Tu, C. Tian, J. Geng, Z. Lin and Z. Dang, *Environ. Pollut.*, 2018, **235**, 11–19.
98 S. Shi, Q. Dong, Y. Wang, X. Zhang, S. Zhu, Y. T. Chow, X. Wang, L. Zhu, G. Zhang and D. Xu, *Sep. Purif. Technol.*, 2021, **266**, 118584.
99 J. Jia, X. Du, Q. Zhang, E. Liu and J. Fan, *Appl. Surf. Sci.*, 2019, **492**, 527–539.
100 L. Wang, J. Wang, W. Yan, C. He and Y. Shi, *Chem. Eng. J.*, 2020, **387**, 123305.
101 I. A. Kumar and N. Viswanathan, *J. Taiwan Inst. Chem. Eng.*, 2019, **102**, 283–296.
102 H. Luo, H. Rong, T. C. Zhang, X. Zeng and J. Wan, *J. Appl. Polym. Sci.*, 2019, **136**, 46897.
103 J. Sun, Y. Chen, H. Yu, L. Yan, B. Du and Z. Pei, *J. Colloid Interface Sci.*, 2018, **532**, 474–484.
104 L. Ai, C. Zhang and L. Meng, *J. Chem. Eng. Data*, 2011, **56**, 4217–4225.
105 R. Li, J. J. Wang, B. Zhou, M. K. Awasthi, A. Ali, Z. Zhang, L. A. Gaston, A. H. Lahori and A. Mahar, *Sci. Total Environ.*, 2016, **559**, 121–129.
106 M. Ebadi, S. Bullo, K. Buskara, M. Z. Hussein, S. Fakurazi and G. Pastorin, *Sci. Rep.*, 2020, **10**, 1–19.
107 G. George and M. Saravanakumar, *Sol. Energy*, 2020, **202**, 144–154.
108 L. He, W. Zhang, X. Zhang, X. Bai, J. Chen, M. Ikram, G. Zhang and K. Shi, *Colloids Surf., A*, 2020, **603**, 125142.
109 Y. Wang, S. Tao, H. Lin, G. Wang, K. Zhao, R. Cai, K. Tao, C. Zhang, M. Sun and J. Hu, *Nano Energy*, 2021, **81**, 105606.
110 R. Syah, A. Al-Khowarizmi, M. Elveny and A. Khan, *Environ. Technol. Innovation*, 2021, **23**, 101805.
111 A. Khenifi, Z. Derriche, C. Mousty, V. Prévot and C. Forano, *Appl. Clay Sci.*, 2010, **47**, 362–371.
112 R.-r. Shan, L.-g. Yan, Y.-m. Yang, K. Yang, S.-j. Yu, H.-q. Yu, B.-c. Zhu and B. Du, *J. Ind. Eng. Chem.*, 2015, **21**, 561–568.
113 Y.-U. Han, C.-G. Lee, J.-A. Park, J.-K. Kang, I. Lee and S.-B. Kim, *Environ. Eng. Res.*, 2012, **17**, 133–138.
114 Y.-U. Han, W.-S. Lee, C.-G. Lee, S.-J. Park, K.-W. Kim and S.-B. Kim, *Desalin. Water Treat.*, 2011, **36**, 178–186.
115 C.-G. Lee and S.-B. Kim, *Environ. Technol.*, 2013, **34**, 2749–2756.
116 N. T. Kim Phuong, *Environ. Technol.*, 2014, **35**, 2829–2836.
117 P. Karthikeyan and S. Meenakshi, *Environmental Chemistry and Ecotoxicology*, 2021, **3**, 42–50.
118 A. Idris, E. Misran, N. Hassan, A. Abd Jalil and C. E. Seng, *J. Hazard. Mater.*, 2012, **227**, 309–316.
119 X. Li, C. Wang, J. Zhang, J. Liu, B. Liu and G. Chen, *Sci. Total Environ.*, 2020, **711**, 134847.
120 W. Gwenzi, N. Chaukura, C. Noubactep and F. N. Mukome, *J. Environ. Manage.*, 2017, **197**, 732–749.
121 S. Salehi and M. Hosseinifard, *Cellulose*, 2020, **27**, 8859–8883.
122 L. Zhang, L. Wan, N. Chang, J. Liu, C. Duan, Q. Zhou, X. Li and X. Wang, *J. Hazard. Mater.*, 2011, **190**, 848–855.
123 X. Cui, X. Dai, K. Y. Khan, T. Li, X. Yang and Z. He, *Bioresour. Technol.*, 2016, **218**, 1123–1132.
124 Y. Zhu, S. Murali, W. Cai, X. Li, J. W. Suk, J. R. Potts and R. S. Ruoff, *Adv. Mater.*, 2010, **22**, 3906–3924.
125 G. Z. Kyzas, E. A. Deliyanni and K. A. Matis, *J. Chem. Technol. Biotechnol.*, 2014, **89**, 196–205.
126 I. Aswin Kumar, M. Naushad and N. Viswanathan, *J. Chem. Eng. Data*, 2020, **65**, 2712–2724.
127 I. A. Kumar, M. Naushad, T. Ahamad and N. Viswanathan, *Int. J. Biol. Macromol.*, 2021, **170**, 13–23.
128 S. Shan, H. Tang, Y. Zhao, W. Wang and F. Cui, *Chem. Eng. J.*, 2019, **359**, 779–789.
129 J. Wan, C. Zhu, J. Hu, T. C. Zhang, D. Richter-Egger, X. Feng, A. Zhou and T. Tao, *Appl. Surf. Sci.*, 2017, **423**, 484–491.
130 E. Platero, M. E. Fernandez, P. R. Bonelli and A. L. Cukierman, *J. Colloid Interface Sci.*, 2017, **491**, 1–12.
131 Y. Gu, D. Xie, Y. Ma, W. Qin, H. Zhang, G. Wang, Y. Zhang and H. Zhao, *ACS Appl. Mater. Interfaces*, 2017, **9**, 32151–32160.
132 C.-M. Hung, C.-P. Huang, C.-W. Chen, C.-H. Wu, Y.-L. Lin and C.-D. Dong, *Environ. Pollut.*, 2020, **265**, 114914.
133 K. N. Palansooriya, S. Kim, A. D. Igalavithana, Y. Hashimoto, Y.-E. Choi, R. Mukhopadhyay, B. Sarkar and Y. S. Ok, *J. Hazard. Mater.*, 2021, **415**, 125464.
134 H. Zhang, C. Chen, E. M. Gray and S. E. Boyd, *Biomass Bioenergy*, 2017, **105**, 136–146.
135 N. Chaukura, R. Chiworeso, W. Gwenzi, M. M. Motsa, W. Munzeiwa, W. Moyo, I. Chikurunhe and T. T. Nkambule, *Appl. Clay Sci.*, 2020, **185**, 105409.
136 K.-W. Jung, T.-U. Jeong, H.-J. Kang and K.-H. Ahn, *Bioresour. Technol.*, 2016, **211**, 108–116.
137 S. E. Hale, V. Alling, V. Martinsen, J. Mulder, G. D. Breedveld and G. Cornelissen, *Chemosphere*, 2013, **91**, 1612–1619.
138 K.-W. Jung, K. Kim, T.-U. Jeong and K.-H. Ahn, *Bioresour. Technol.*, 2016, **200**, 1024–1028.
139 P. Bonelli, P. Della Rocca, E. Cerrella and A. Cukierman, *Bioresour. Technol.*, 2001, **76**, 15–22.
140 N. Y. Acelas, S. M. Mejia, F. Mondragón and E. Flórez, *Comput. Theor. Chem.*, 2013, **1005**, 16–24.

141 Y. Zhao, L. Gai, H. Liu, Q. An, Z. Xiao and S. Zhai, *Int. J. Biol. Macromol.*, 2020, **162**, 301–309.
142 J. Xie, L. Lai, L. Lin, D. Wu, Z. Zhang and H. Kong, *J. Environ. Sci. Health, Part A: Toxic/Hazard. Subst. Environ. Eng.*, 2015, **50**, 1298–1305.
143 Y. Zhang, B. Pan, C. Shan and X. Gao, *Environ. Sci. Technol.*, 2016, **50**, 1447–1454.
144 L. Fang, B. Wu, J. K. Chan and I. M. Lo, *Chemosphere*, 2018, **192**, 209–216.
145 C.-C. Fu, H. N. Tran, X.-H. Chen and R.-S. Juang, *J. Ind. Eng. Chem.*, 2020, **83**, 235–246.
146 H. Luo, X. Zeng, P. Liao, H. Rong, T. C. Zhang, Z. J. Zhang and X. Meng, *Int. J. Biol. Macromol.*, 2019, **126**, 1133–1144.
147 P. Hu, Q. Liu, J. Wang and R. Huang, *Polym. Eng. Sci.*, 2017, **57**, 44–51.
148 D. Wu, Y. Gao, W. Li, X. Zheng, Y. Chen and Q. Wang, *ACS Sustainable Chem. Eng.*, 2016, **4**, 6732–6743.
149 B. Yang, D. Xu, X. Wu, Z. Li, L. Lei and X. Zhang, *J. Ind. Eng. Chem.*, 2015, **25**, 67–72.
150 B. K. Biswas, J.-i. Inoue, K. Inoue, K. N. Ghimire, H. Harada, K. Ohto and H. Kawakita, *J. Hazard. Mater.*, 2008, **154**, 1066–1074.
151 B. Wang, W. Zhang, L. Li, W. Guo, J. Xing, H. Wang, X. Hu, W. Lyu, R. Chen and J. Song, *Chemosphere*, 2020, **256**, 127124.
152 B. Wang, W. Zhang, L. Li, W. Guo, J. Xing, H. Wang, X. Hu, W. Lyu, R. Chen, J. Song, L. Chen and Z. Hong, *Chemosphere*, 2020, **256**, 127124.
153 K.-W. Jung, T.-U. Jeong, J.-W. Choi, K.-H. Ahn and S.-H. Lee, *Bioresour. Technol.*, 2017, **244**, 23–32.
154 R. Sujitha and K. Ravindhranath, *J. Anal. Methods Chem.*, 2017, **2017**, 3610878.
155 S. El-Gawad and H. El-Aziz, *MOJ Biol. Med.*, 2018, **3**, 227–236.
156 P. Karthikeyan, H. A. T. Banu and S. Meenakshi, *Int. J. Biol. Macromol.*, 2019, **130**, 407–418.
157 H. Siwek, A. Bartkowiak, M. Włodarczyk and K. Sobecka, *Water, Air, Soil Pollut.*, 2016, **227**, 427.
158 G. Mohan, A. N. Babu, K. Kalpana and K. Ravindhranath, *Asian J. Chem.*, 2017, **29**, 2549–2558.
159 W. K. Biftu and K. Ravindhranath, *Water Sci. Technol.*, 2020, **81**, 2617–2633.
160 X. Ji, D. Wu, Y. Wang, L. Ge, W. Hong, R. Xue and B. Wang, *RSC Adv.*, 2015, **5**, 55191–55200.
161 Z. Mahmood, S. Nasir, N. Jamil, A. Sheikh and A. Akram, *Afr. J. Environ. Sci. Technol.*, 2015, **9**, 274–281.
162 H. Yang, Q. Zhou, W. Luo, C. Yan and C. Zhou, *Desalin. Water Treat.*, 2016, **57**, 18354–18365.
163 H. Luo, X. Zeng, P. Liao, H. Rong, T. C. Zhang, Z. Jason Zhang and X. Meng, *Int. J. Biol. Macromol.*, 2019, **126**, 1133–1144.
164 A. Zhou, C. Zhu, W. Chen, J. Wan, T. Tao, T. C. Zhang and P. Xie, *Colloids Surf., A*, 2018, **554**, 237–244.
165 T. Almeelbi, M. Haugstad and A. Bezbaruah, Aqueous phosphate removal using bare and Ca-alginate entrapped nanoscale zero-valent iron, in *World Environmental and Water Resources Congress 2011: Bearing Knowledge for Sustainability*, 2011, pp. 1733–1740, https://doi.org/10.1061/41173(414)180.